Engineering Science and Technology, an International Journal 19 (2016) 1635–1654

HOSTED BY

Contents lists available at ScienceDirect

Engineering Science and Technology, an International Journal

journal homepage: www.elsevier.com/locate/jestch

Full Length Article

# Quasi-oppositional differential search algorithm applied to load frequency control

Dipayan Guha [a,*], Provas Kumar Roy [b], Subrata Banerjee [c]

[a] Department of Electrical Engineering, Dr. B.C. Roy Engineering College, Durgapur, West Bengal, India
[b] Department of Electrical Engineering, Jalpaiguri government Engineering College, Jalpaiguri, West Bengal, India
[c] Department of Electrical Engineering, NIT-Durgapur, Durgapur, West Bengal, India

ARTICLE INFO

*Article history:*
Received 14 July 2016
Revised 2 September 2016
Accepted 26 September 2016
Available online 5 October 2016

*Keywords:*
Load frequency control
Differential search algorithm
Quasi-oppositional based learning
Generation rate constraint
Governor dead band
Transient analysis
Sensitivity analysis

ABSTRACT

In this article, quasi-oppositional differential search algorithm (QODSA) is proposed for finding an optimal and effective solution for load frequency control (LFC) problem in the power system. Initially, original DSA is employed for fine-tuning of the secondary controller of LFC system and then, quasi-oppositional based learning (Q-OBL) mechanism is integrated into the original DSA to enhance the convergence speed and to find a better solution of LFC problem. To validate the effectiveness of proposed QODSA, four widely used interconnected power system networks are designed and analyzed. The superiority of the proposed method is established by an extensive comparative analysis with other existing evolutionary algorithm's (EA) using transient analysis method. A critical investigation of simulation results reveals that the proposed QODSA gives simple and better solution compared to original DSA and other reported algorithms. To study the robustness of QODSA, two different random load patterns are projected and results confirm the robustness of the designed controllers. To add some degree of nonlinearity, generation rate constraint and governor dead band effects are considered and their consequence on the system dynamics has been examined. Finally, sensitivity analysis is performed with a wide variation of system parameters.


## 1. Introduction

The main idea of power system operation and control is to maintain an electric energy system to its equilibrium condition so that uninterrupted power can be delivered to the customers. This can be achieved by keeping system frequency and terminal voltage profiles to their nominal levels. In this context, two techniques are normally employed in power system. One is used to control the mechanical input power to the electrical generator so that active power and output frequency of the same can be controlled and another is about the control of reactive power and terminal voltage. The control of frequency and active power is referred to as load frequency control (LFC). Stabilization of area frequency and tie-line power oscillation caused by the step load perturbation (SLP) is the most challenging issue in power system operation and control and it received significant attention in LFC study [1–2]. The advanced power system networks are made up with several control areas and in each controlled area, LFC is used to monitor the error in frequency and tie-line power flow. Accordingly it compute the net change (generally named as area control error, ACE) in power generation is required to match the load demand. ACE is defined as a linear combination of frequency and tie-line power flow and used to show the deficiency or excess of power generation at any instant of time. The main objective of LFC is to nullify the ACE so that both frequency and tie-line power error can approaches to zero [3–4].

Several approaches for control and optimization like classical [1–8], optimal [9], robust [10], fractional order [11], fuzzy logic [12,13], artificial neural network [14–16], variable structure controller [17], adaptive control [18–20], fuzzy wavelet neural network [21], adaptive backstepping [22] etc. have been reported in the literature over the past two-three decades to enhance the degree of transient and steady-state stability of power system. In [23], authors have discussed global transient's stability and voltage regulation for power system. The control strategy employed in LFC system is not only used to maintain the constancy in frequency and tie-line power flow but also accomplishes zero steady state error and accidental interchanges. Among the aforesaid controllers, classical controllers in the form of proportional-integral (PI) and/or proportional integral derivative (PID) are quite in vogue because of its structural simplicity, ease realization, low cost, robust perfor-

* Corresponding author.
*E-mail address:* guha.dipayan@yahoo.com (D. Guha).
Peer review under responsibility of Karabuk University.

http://dx.doi.org/10.1016/j.jestch.2016.09.021
2215-0986/

mance, shows better dynamic performance irrespective to the parameter variation etc. [17,24].

Usually, a linear model around the nominal operating point is used for LFC design. Because of the nonlinear, time-varying nature of the power system and inherent characteristic of the load, the operating point of the power system is continuously varying during a daily cycle. Therefore, the controller design at fixed operating point may not be able to give acceptable performance in another status. This encourages the present researchers to find an effective optimization method for the optimal design of supplementary controller in LFC system. Literature survey reveals that a number of optimization methods like bacterial foraging optimization algorithm (BFOA) [1,6], particle swarm optimization (PSO) [5], firefly algorithm (FA) [2], hybrid BFOA-PSO (hBFOA-PSO) [3], differential evolution (DE) [4,13], teaching learning based optimization (TLBO) [7], biogeography based optimization (BBO) [8], imperialist competitive algorithm [10], tabu search algorithm (TSA) [16], bat inspired algorithm (BIA) [24], backtracking search algorithm (BSA) [25], gravitational search algorithm (GSA) [26], improved PSO [27] etc. have been already applied to the LFC area over the past few decades for betterment of the system stability. Padhan et al. have demonstrated FA in [2] and compared its performance with BFOA, hBFOA-PSO, DE, GA, and conventional controllers for the similar interconnected power system. In [8], an optimal classical controller and superconducting magnetic energy storage (SMES) based frequency stabilizer were designed and implemented employing BBO method for an interconnected nonlinear power system and established the superiority of BBO over the other reported intelligent controllers. Variable structure controller (VSC) applied to LFC system is available in [16] and TSA was proposed to find optimal feedback gain and switching vector of VSC. An improved PSO algorithm is presented in [27] for optimal design of thyristor control series capacitor (TCSC) and transient responses validated that coordinated LFC-TCSC controller provide better damping to the system oscillations caused by the load perturbation. Sahib in [28] has demonstrated PSO for the optimal design of PID with double derivative controller and applied to automatic voltage regulator. The effectiveness of redox flow batteries and interline power flow controller in LFC area has been discussed in [29] and the gains of the optimal controller are searched by DE algorithm. Pradhan et al. [30] have proposed SMES and unified power flow controller (UPFC) in coordination with fuzzy PID controller to accelerate the degree of relative stability of power system. Recently, quasi-oppositional harmony search algorithm (QOHSA) has been discussed in [31] for multi-area multi-unit power system under the deregulation environment. The tuning ability and advantage of grey wolf optimization (GWO) algorithm to cope up with interconnected power system under the normal and perturbed scenario has been enumerated in [32,33].

However, the problem associated with the aforementioned techniques is that they suffer from poor convergence rate and low exploitation ability. Additionally, the performance of the aforesaid optimization techniques is highly determined by some of their input control parameters. For example, the performance of PSO algorithm is highly susceptible to the initial value of weighting factor of the cognitive and social components, and weighting strategy of the velocity vector. The search ability of DE is highly controlled by the mutation factor (F) and crossover rate (CR). In case of HAS, determination of harmony memory search, harmony memory consideration rate, the distance bandwidth, pitched adjusting factor, and number of improvisation is obligatory. In BFOA, during the chemotactic process, the performance of the algorithm is highly determined by the random search direction that may leads to delay to reach the global optimal point. Additionally, the no. of search agents involve in the BFOA is higher than GA and, hence, the possibility of getting suboptimal solution is more in BFOA. The input parameters of GSA are: initial gravitational constant ($G_0$), total no. of agents ($K_0$), and a constant $\alpha$. Firefly algorithm (FA) is controlled by mainly three parameters, namely randomization parameter ($\alpha$), the attractiveness ($\beta$), and the absorption coefficient ($\gamma$).

Further, in the line of "**no-free-lunch**" theorem, there is no optimization technique which is well defined for all type of optimization problems. This motivate us to propose a new algorithm, especially input control parameters free, with the hope to solve a wider range of unsolved problem. Therefore, it is justified to propose a new optimization method to explore the LFC performance so as to ameliorate the degree of stability of power system. The main motivation for the expansion of differential search algorithm (DSA) is to achieve a simpler and effective solution of LFC problem. DSA is a recently introduced population based stochastic optimization method proposed by Civicioglu in 2012, which is inspired by the *Brownian-like-random-walk* used by an organism to migrate [34]. It is an iterative process which tries to minimize the selected objective function. Additionally, authors have introduced quasi-oppositional based learning (QOBL) mechanism into the original DSA to accelerate the convergence speed and to improve the computational efficiency of same. The proposed quasi-oppositional DSA (QODSA) method is tested on four well-known interconnected power systems and established its superiority over some recently published control algorithms for the identical test system by the transient analysis method. Two types of random load perturbation (RLP) are projected in this article to verify the robustness of the designed controllers. Finally, parametric uncertainties are considered for sensitivity analysis of the designed controllers.

Rest of the article is organized as follows: Section 2 explains the mathematical model of test system followed by the definition of the fitness function. In Section 3, the proposed method, i.e. original DSA and QODSA, is briefly elaborated. Section 3 also gives the algorithmic steps of QODSA applied to LFC problem. Experimental verification including transient responses is described in Section 4. Concluding remarks is available in Section 5.

## 2. Problem formulation

To evaluate the performance of QODSA, four widely employed interconnected power systems viz. two-area non-reheat thermal power plant [1–4], three-area thermal power plant [2], two-area multi-source multi-unit power plant [35] and five-area thermal power plant [36] are considered for the present study. Firstly, a two-equal area non-reheat thermal power plant (test system 1) with 2000 MW capacity each is designed and analyzed. The classical controllers, i.e., PI and PID, are employed in the test system as a secondary controller. It is noted that for the sake of best possible generation, it is needed to utilize a distinct controller for each generating unit. Fig. 1 illustrates the linearized transfer function model of the concerned power system and 10% SLP in area-1 is considered for the assessment of transient responses. The system parameters are taken from [2] and presented in Appendix. In Fig. 1, $T_g$ is the time constant of speed governor, $T_t$ is the time constant of steam turbine, $K_{ps}$ is the gain of power system unit, $T_{ps}$ is time constant of power system unit, $B_1$ and $B_2$ are the frequency bias parameter of area-1 and area-2, respectively, $R_1$ and $R_2$ are the speed regulation parameter of speed governor in area-1 and area-2, respectively, $T_{12}$ is the synchronizing time constant of tie-line, $\Delta P_D$ is the load disturbance, $\Delta f_1$ and $\Delta f_2$ are deviation of frequency in area-1 and area-2, respectively, $\Delta P_{tie}$ is the deviation of tie-line power. Furthermore, to perform the study in realistic scenario, appropriate value of GRC (3% min) and governor dead band nonlinearities are included in the system modeling and their impact on the system dynamics has been inspected.

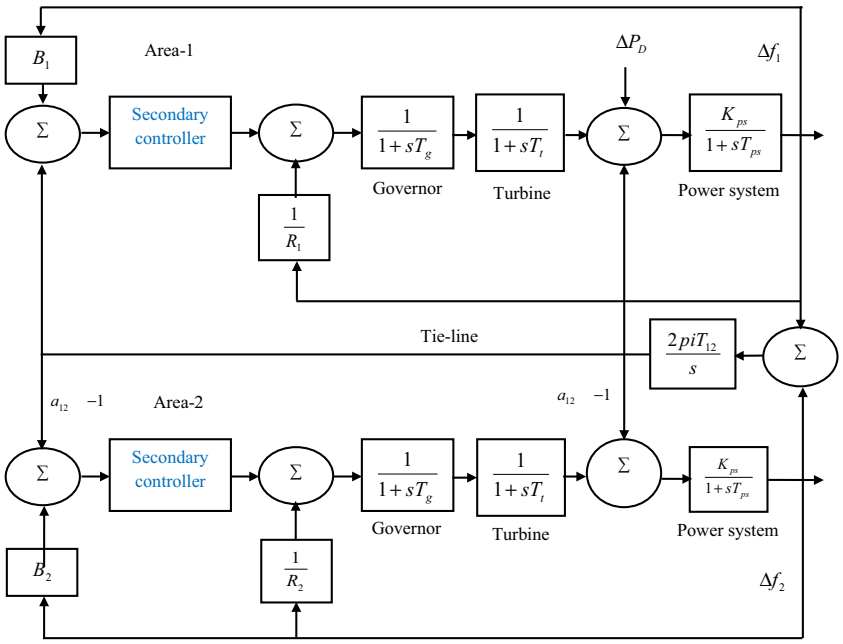


**Fig. 1.** Block diagram of two-area interconnected non-reheat thermal-thermal power system.

To verify the feasibility of proposed algorithm, the study is extended to three more test systems and critical analysis of their dynamic behavior is presented and discussed in the following headings. Three unequal all thermal power plant (test system-2) [2], two-area multi-unit multi-source power plant (test system-3) [35], and five-area thermal power plant [36] are simulated and controller gains are simultaneously optimized by the proposed QODSA.

For the optimal design of secondary controllers, ACE of the respective area is considered as an input ($e_1$, $e_2$) to the controller and controlled inputs ($u_1$, $u_2$) to the plant with PI/PID controller action can be defined by (1) and (2).

$$\left.\begin{aligned} u_1 &= K_{p1}(ACE_1) + K_{i1}\int_{t=0}^{t}(ACE_1)dt \\ u_2 &= K_{p2}(ACE_2) + K_{i2}\int_{t=0}^{t}(ACE_2)dt \end{aligned}\right\}\text{For PI-controller} \quad (1)$$

$$\left.\begin{aligned} u_1 &= K_{p1}(ACE_1) + K_{i1}\int_{t=0}^{t}(ACE_1)dt + K_{d1}\frac{d}{dt}(ACE_1) \\ u_2 &= K_{p2}(ACE_2) + K_{i2}\int_{t=0}^{t}(ACE_2)dt + K_{d2}\frac{d}{dt}(ACE_2) \end{aligned}\right\}\text{For PID-controller} \quad (2)$$

In an optimal control system design, the fitness function or objective function is selected (i) either by taking the few points of the time response or (ii) by taking the entire time response, named as **integral criterion**. The commonly used integral criterions are integral square error (ISE), integral time square error (ITSE), integral absolute error (IAE), and integral time absolute error (ITAE). ISE exhibits smaller overshoot but albeit large settling time. IAE is often used where digital simulation is employed. Further, it produces slower response. ITSE and ITAE has an additional time multiplier of the error function, which highlight long duration errors and gives faster time response compared to ISE and IAE. ITSE criterion based controller offers large controller output for the sudden change in reference value, which is not wanted from the controller design point of view. ITAE weight the errors which exist after a long time much more heavily than those at the beginning of the response. ITAE based tuning makes the system to settle down much faster than the other said tuning methods. ITAE criterion also provides minimum peak overshoot. Inspired from the above discussion, ITAE based performance index is considered in this article for fine tuning of the proposed controllers. It is further reported in [2] that ITAE based objective function gives the improved result in LFC area. Therefore, the objective function based on ITAE criterion is defined as follows:

$$J = \int_{t=0}^{\infty}\{abs(\Delta f_1) + abs(\Delta f_2) + abs(\Delta P_{tie})\} * t * dt \quad (3)$$

The design LFC problem can be viewed as a constraint optimization problem, which is limited by the controller settings. Thus, the constraint LFC problem can be defined as follows:Minimize $J$:

$$\text{Subjected to : } \left.\begin{aligned} K_{p,\min} \leqslant K_p \leqslant K_{p,\max} \\ K_{i,\min} \leqslant K_i \leqslant K_{i,\max} \end{aligned}\right\}\text{For PI-controller}$$

$$\left.\begin{aligned} K_{p,\min} \leqslant K_p \leqslant K_{p,\max} \\ K_{i,\min} \leqslant K_i \leqslant K_{i,\max} \\ K_{d,\min} \leqslant K_d \leqslant K_{d,\max} \end{aligned}\right\}\text{For PID-controller}$$

where $K_{pid,\min}$ and $K_{pid,\max}$ are the minimum and the maximum limits of PID-controller parameters and optimally selected between [−2, 2], respectively [2].

## 3. Optimization technique

Recently, meta-heuristic optimization algorithms have been widely employed for solving complex, nonlinear optimization problems. These are found to be efficient and give optimum solutions nearer to the global value than that of conventional methods. They involve two operators for searching the optimum solution within the defined search space namely intensification and diversification. Intensification phase searches the best solutions around the current solutions and diversification ensure that the algorithm reach the optimum solution efficiently [37]. In this section, initially, the motivation of original DSA in context to LFC problem is elaborated and afterward, the theory of oppositional based learning (OBL) followed by the quasi-opposite number is demonstrated.

### 3.1. Differential search algorithm (DSA)

DSA is a relatively new population-based heuristic evolutionary algorithm (EA) developed by Civicioglu [34]. It is inspired by the migration process of a living organism which constitutes superorganism during climate change of the year. Migration process allows species to move from a habitat to more efficient habitat where capacity and diversity of natural resources are more. The movement of superorganism can be characterized by *Brownian-like-random-walk model* [34]. In DSA, the search space is simulated as a food area and each location in the search space represents an artificial superorganism. DSA initiates with random initialization of artificial superorganism ($X_{i,j}$) of $[N_p * D]$ dimension within the search space using (4).

$$X_{i,j} = low_j + rand * (up_j - low_j) \text{ where } i = 1, 2, - - -, N_p \text{ and } j = 1, 2, \ldots, D \quad (4)$$

where $N_p$ signifies the number of elements in the superorganism (population size) and $D$ indicates the dimension of the problem, i.e. number of control variables, *up* and *low* defines the upper and lower bounds of the solution space, respectively.

After initialization, *stopover vector* in the search area is randomly generated by random shuffling which is essential for successful implementation of the migration process in DSA. Stopover vector ($S_{i,G}$) can be computed using (5).

$$S_{i,G} = X_{i,G} + scale * (donor - X_{i,G}) \quad (5)$$

where

$$scale = randg(2 * rand_1) * (rand_2 - rand_3) \quad (6)$$

and

$$donor = X_{i,j}|_{random\_shuffling} \quad (7)$$

The *scale* controls the size of the change in the positions of the individual of the artificial organism, *randg* is a random value chosen from a gamma distribution and $rand_1$, $rand_2$, $rand_3$ are the random numbers selected between [0, 1].

The search process of stopover vector can be calculated by the individual organism of the superorganism using the following process [38]:

$$S'_{i,j,G} = \begin{cases} S_{i,j,G} \\ X_{i,j,G} \end{cases} if \begin{cases} r_{i,j} = 0 \\ r_{i,j} = 1 \end{cases} \quad (8)$$

where $S'_{i,j,G}$ defines the trial vector of *jth* the particle in the *ith* dimension at the *Gth* generation and $r_{i,j}$ is an integer either 1 or 0.

The selection operation is used to define the next generation, i.e. $G = G + 1$, between *stop over vector* population and *artificial organism* population based on the fitness value. The selection operation is described as follows:

$$X_{i,G+1} = \begin{cases} S_{i,G} \\ X_{i,G} \end{cases} if \begin{cases} f(S'_{i,G}) \leqslant f(X_{i,G}) \\ f(S'_{i,G}) > f(X_{i,G}) \end{cases} \quad (9)$$

For more details about DSA, readers are referring to [34].

### 3.2. Quasi-oppositional based learning (Q-OBL)

EA's are well-known methods to cope nonlinear, complex optimization problem. However, it suffers from long computational time due to the natural behavior of EA's, especially when the solution space is difficult to explore [39]. DSA has good exploring power in the search space and locating the region of global optimum solutions, however, it suffers from low convergence rate. Oppositional based learning (OBL) method is applied to DSA to accelerate the convergence speed and to improve the computational efficiency of the same. According to probability theorem, in 50% of cases the random initialization of candidate solution is farther from global solution than opposite guess, thus opposite guess can effectively reduce search space area and improve convergence speed. While evaluating a solution ($x$) to a given problem, simultaneously its opposite number ($x^0$), is also estimated to achieve a better approximation of candidate solution.

Mathematically, the value of $x^0$ in one dimensional and $d$-dimensional search space can be found using (10) and (11), respectively.

$$x^0 = a + b - x \quad (10)$$

$$x_i^0 = a_i + b_i - x_i \qquad \forall i = 1, 2, \ldots, d \quad (11)$$

where $a$ and $b$ are the minimum and maximum limits of the search space. Let, $P(x_1, x_2, \ldots, x_n)$ be a point in a $d$-dimensional search space with $x_i \in (a_i, b_i)$ $\forall i = 0, 1, 2, \ldots, d$ be the candidate solution. Assuming $f(x)$ is the fitness value measured the optimality of candidate solution. An opposite solution of $P$ can be defined as $P^0(x_1^0, x_2^0, \ldots, x_d^0)$ using (11). If, fitness value $f^0(x)$ obtained with $P^0$ is better than the value obtained with $P$, then replace $P$ by $P^0$, otherwise keep $P$ as the current solution.

It is further noted from the literature that quasi-opposite number has a higher probability to be closer to the global solution than the opposite number without any priori information [40]. The quasi-opposite number is created from the interval between the median and opposite number of present population. Mathematically, quasi-opposite number ($x_i^{q0}$) is defined as follows:

$$x_i^{q0} = rand(c_i, x_i^0) \qquad \forall i = 1, 2, \ldots, d \quad (12)$$

where, $c_i = \frac{a_i + b_i}{2}$ and *rand* is a uniformly distributed random number between $[c_i, x_i^0]$. The general flowchart of DSA with Q-OBL is shown in Fig. 2(a).

### 3.3. Algorithmic steps of QODSA applied to LFC

In QODSA, opposite populations of current generations are simultaneously defined within the search space and best candidate solution among them is sorted based on the fitness value and quasi-oppositional jumping rate. The different steps of QODSA for searching an optimal solution of LFC in power system are described as follows:

**Step 1** Initialize the input parameters, i.e., population size ($N_p$), maximum generation count, number of control variables ($D$), upper and lower bounds of controller gains.
**Step 2** Randomly generate an artificial organism, i.e. controller parameters ($K_p, K_i, K_d$) of $[N_p * D]$ dimension within the defined solution space and calculate the fitness value with current population using (3).
**Step 3** Generate quasi-opposite population using (11) and (12). Evaluate fitness value with quasi-opposite population using (3).
**Step 4** Select finest $N_p$ candidate solution between the current generation and quasi-opposite generation based on fitness value computed in step 2 and 3.
**Step 5** Filtered out some elite solution and non-elite solutions are updated by the proposed method.
**Step 6** Perform random shuffling on selected individual member from initial population (*super organism*) and moving towards the target *donor* using following pseudo code:

```
for j = 1 : D, sup erorganism = sup erorganism(:, j);
    for i = 1 : N, w = ⌈rand * i⌉; t = sup erorganism(w);
        sup erorganism(w) = sup erorganism(i);
        sup erorganism(i) = t;
    end
    donor(:, j) = X;
end
```

**Step 7** *Scale* value and *stopover site* are determined using (5), (6), and (7) for successful completion of the migration process.
**Step 8** Set two control variables, $p_1 = 0.3 * rand$ and $p_2 = 0.3 * rand$. Update *stopover site* by random selection process taking the individual member from *super organism*.
**Step 9** Check whether any member of *stopover site* goes beyond the *habitat* (search space) or not using boundary condition of DSA as defined in [34] and accordingly update *stopover site*.
**Step 10** Use quasi-oppositional jumping rate ($J_r$) to generate quasi-opposite solutions and compute the fitness value by (3).

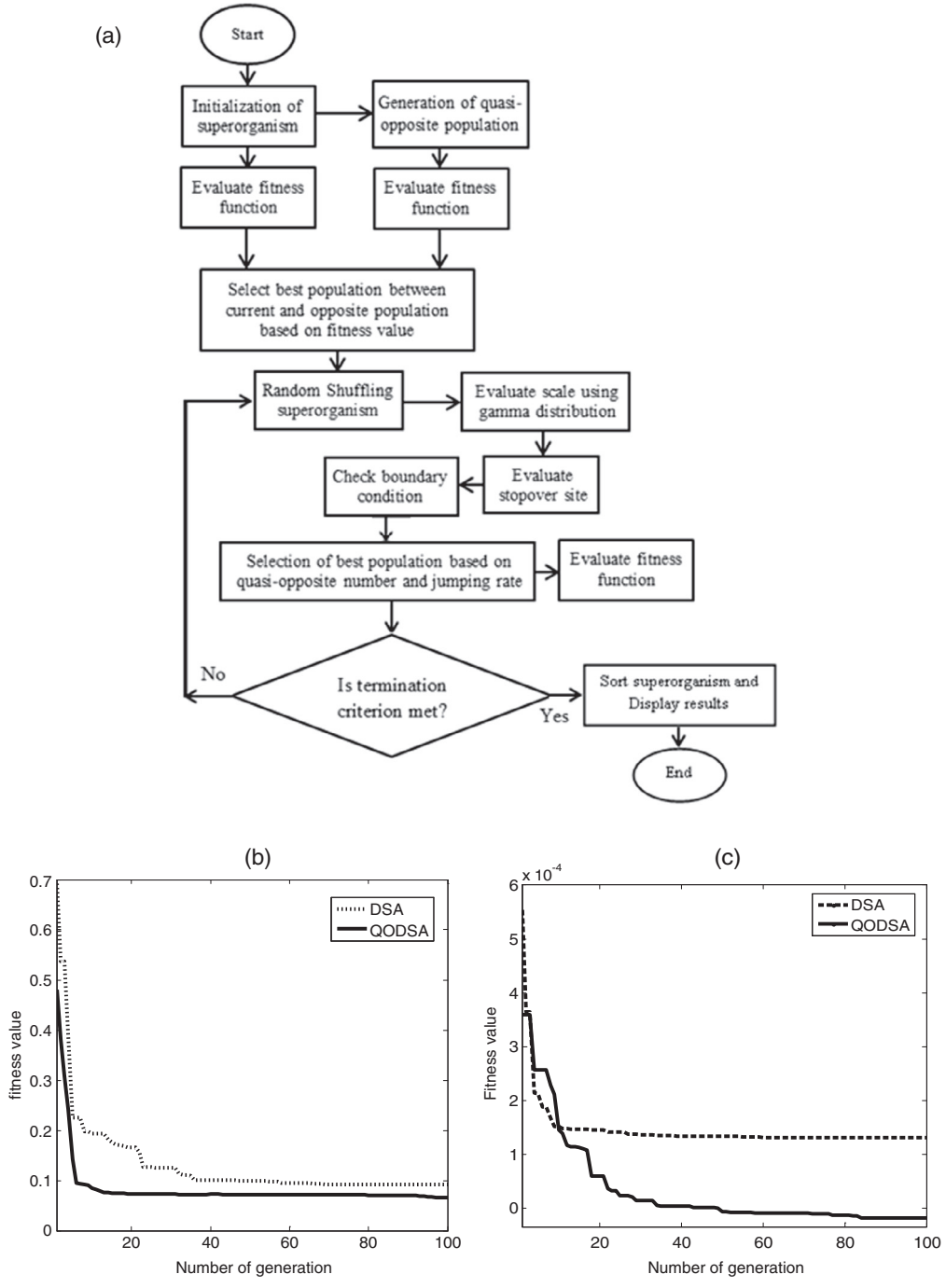


**Fig. 2.** (A) Flowchart of the proposed QODSA algorithm. Comparative convergence characteristics of the proposed algorithm, (b) test system-1, (c) test system-4.

```
if rand < J_r
    for i = 1 : N_p
        for j = 1 : D
            QOP_{i,j} = rand( (a_j + b_j)/2 , OP_{i,j} );
        end
    end
end
```

**Step 11** Select $N_p$ fittest solution from current generation and quasi-oppositional generation based on their fitness value and used them for next iteration.

**Step 12** If the termination criterion is satisfied, then stop iteration and show results to compute transient specifications of the defined system, otherwise go to step 6 for next generation.

## 4. Simulation results and comparative analysis

The main objective of LFC is to reduce the frequency deviation of the individual area as well as the fluctuation of tie-line power flow between the relative areas caused by sudden load perturbation. To ensure the efficiency of proposed QODSA, four different power system networks are considered for the present study. Classical PI/PID controllers are used as a secondary controller and their gains are simultaneously optimized by the proposed methods (DSA and QODSA). Simulation is performed in an Intel core i-3 processor, 2.4 GHz, 4 GB RAM computer in Matlab R2009 (7.8.0) environment. Owing to the randomness of EA's, proper initialization of input parameters is essential to ensure better convergence of same; otherwise, solutions will trap to the local minima. After several trials, following parameters are found to be best for successful implementation of DSA in LFC problem, these are: size of superorganism ($n_P$) = 40, number of problem specific control variables = 6, low habitat limit = −2, upper habitat limit = 2, elite parameter = 4, maximum number of generation = 100.

Initially, original DSA is designed to tune controller parameters and then the theory of Q-OBL is applied to DSA in order to increase the convergence speed and computational efficiency of the same. Comparative convergence profile of DSA and QODSA is shown in Fig. 2(b). It is seen from Fig. 2(b) that QODSA has the higher degree of convergence than original DSA and reaches the global optimum solutions without any unexpected oscillation. The maximum number of iteration is set to 100 for both DSA and QODSA. It seems from Fig. 2(b) that proposed algorithms converge to the optimum solution within 70–80 iteration thus justifying the choice of the maximum number of iteration of 100.

### 4.1. Test system 1

#### 4.1.1. With PI-controller

Primarily, the linear model of two equal area non-reheat type thermal power plant [1–4] including PI-controller is developed and 10% SLP in area-1 is considered for the study. PI-controller gains are simultaneously optimized by the proposed DSA and QODSA via the minimization of (3). The optimum controller settings and other performance indices like minimum ITAE value, settling time of frequency and power oscillations are given in Table 1. In order to make fair comparison between QODSA and other EA's like DSA, FA [2], hBFOA-PSO [3], PSO [3], DE [4], BFOA [1], GA [1], conventional method [1], the dynamic responses of each controller is obtained and depicted in Table 1. The changes of frequency in area-1, area-2, and tie-line power flow after 10% SLP in area-1 with proposed methods and FA [2] are illustrated in Fig. 3. Critical observation of Table 1 reveals that minimum ITAE value is obtained with QODSA (**ITAE = 0.2820**) compare to DSA (ITAE = 0.3299) and other EA's as listed in Table 1. Improvement of ITAE value with QODSA is 14.52% (DSA), 67.57% (FA), 76.23% (hBFOA-PSO), 76.77% (PSO), 71.55% (DE), 84.31% (BFOA), 87.45% (GA), and 92.12% (conventional). It is also noted from Table 1 and Fig. 3 that minimum settling time is achieved with QODSA compared to DSA and other EA's as given in Table 1. Hence, it may be concluded from the aforesaid discussion that QODSA provides more optimal controller settings and shows significant improvement in the system stability compared other EAs as listed in Table 1.

#### 4.1.2. With PID-controller

In order to improve the existing results, classical PID-controllers are employed in each control area in lieu of PI-controller and optimum settings are derived by DSA and QODSA. The optimum value of controller parameters obtained with DSA and QODSA are presented in Table 2. The dynamic responses of each controller are obtained and compared with FA based PID controller [2]. The comparative transient responses with PID controller are shown in Fig. 4. The settling time of $\Delta f_1$, $\Delta f_2$, and $\Delta P_{tie}$ are noted down from Fig. 4 and presented in Table 2. Critical observation of Table 2 and Fig. 4 show that QODSA based PID controller gives better results than DSA and FA in terms of minimum fitness value, settling time of $\Delta f_1$, $\Delta f_2$, and $\Delta P_{tie}$. Hence, QODSA may be considered as the finest optimization method and rest of the study is performed with QODSA-tuned PID-controller.

#### 4.1.3. Sensitivity analysis of test system-1

To identify the potentiality and usefulness of proposed QODSA-optimized PID controller, sensitivity analysis is performed with a wide variation of system parameters and loading conditions. The system parameters and loading conditions are changed in the range of ±50% instep of 25% from their nominal settings. The changed parameters are time constant of a speed governor ($T_g$), steam

**Table 1**
Comparative analysis between different optimization techniques with PI-controller structure for test system-1.

| Optimization method | Controller gains | | | | ITAE value | Settling time (sec) | | |
|---|---|---|---|---|---|---|---|---|
| | $K_{i1}$ | $K_{i2}$ | $K_{p1}$ | $K_{p2}$ | | $\Delta f_1$ | $\Delta f_2$ | $\Delta P_{tie}$ |
| Conventional [1] | 0.4741 | 0.4741 | −0.3317 | −0.3317 | 3.5795 | 45 | 45.01 | 28.27 |
| GA [1] | 0.2662 | 0.2662 | −0.2346 | −0.2346 | 2.2475 | 10.59 | 11.39 | 9.37 |
| BFOA [1] | 0.4741 | 0.4741 | −0.3317 | −0.3317 | 1.8379 | 5.52 | 7.09 | 6.35 |
| DE [4] | 0.4335 | 0.4335 | −0.2146 | −0.2146 | 0.9911 | 8.96 | 8.16 | 5.75 |
| PSO [3] | 0.4756 | 0.4756 | −0.3597 | −0.3597 | 1.2142 | 7.37 | 7.82 | 5 |
| hBFOA-PSO [3] | 0.4741 | 0.4741 | −0.3317 | −0.3317 | 1.1865 | 7.39 | 7.65 | 5.73 |
| FA [2] | 0.4296 | 0.4296 | −0.3267 | −0.3267 | 0.8695 | 7.11 | 7.22 | 5.62 |
| DSA | 0.8898 | 0.0037 | −0.2811 | 0.0694 | 0.3299 | 5.95 | 6.85 | 6.12 |
| QODSA | 0.9899 | 0.0032 | −0.2520 | 0.1310 | **0.2820** | **5.50** | **6.43** | **6.09** |

Bold signifies best result.

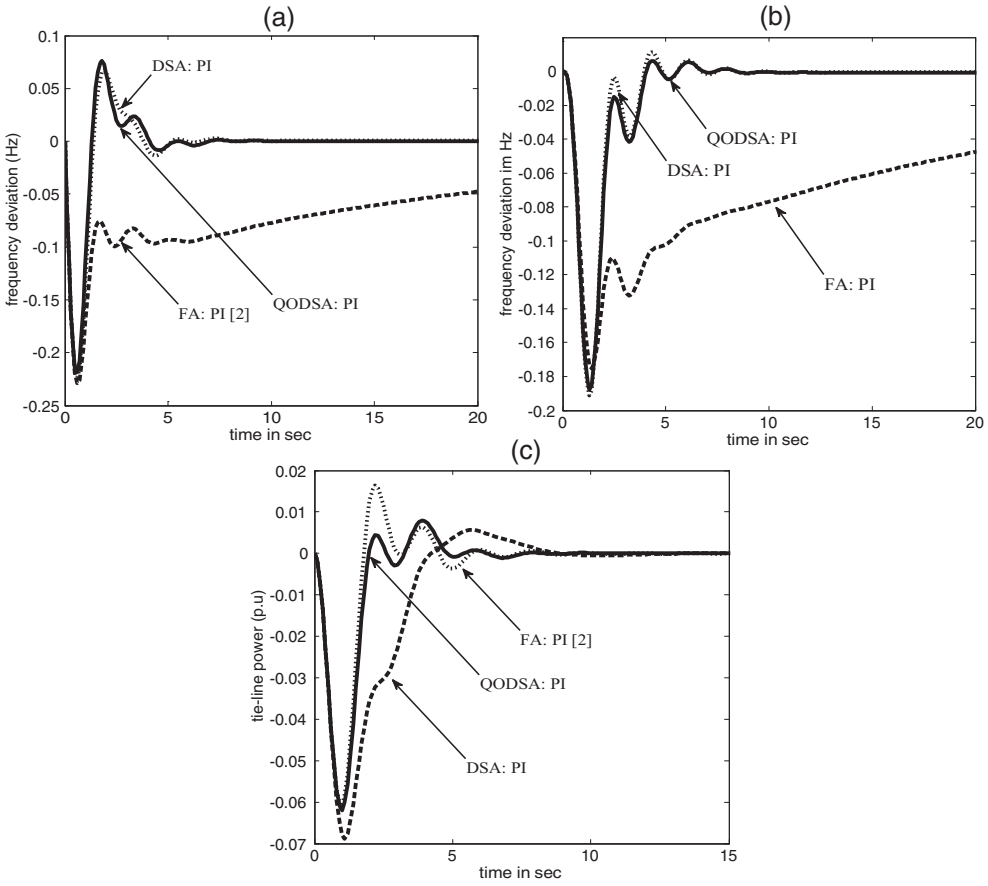


**Fig. 3.** Comparative transient responses of test system-1 after 10% SLP in area-1 with PI-controller, (a) change of frequency in area-1, (b) change of frequency in area-2, (c) change of tie-line power.

**Table 2**
Comparative analysis between different optimization techniques with PID-controller structure for test system-1.

| Optimization method | Controller gains | | | | | | ITAE value | Settling time (sec) | | |
|---|---|---|---|---|---|---|---|---|---|---|
| | $K_{i1}$ | $K_{i2}$ | $K_{p1}$ | $K_{p2}$ | $K_{d1}$ | $K_{d2}$ | | $\Delta f_1$ | $\Delta f_2$ | $\Delta P_{tie}$ |
| FA [2] | 1.0373 | 1.0373 | 1.0556 | 1.0556 | 0.9626 | 0.9626 | 0.4714 | 4.25 | 5.49 | 4.78 |
| DSA | 1.6285 | 0.0790 | 0.5670 | 1.9609 | 0.2630 | 0.7097 | 0.0918 | 2.09 | 2.85 | 2.93 |
| QODSA | 1.9524 | 0.0578 | 0.8246 | 1.9968 | 0.2630 | 0.4588 | **0.0664** | **1.72** | **2.75** | **2.92** |

Bold signifies best result.

turbine ($T_t$), power system itself ($T_{ps}$) and transmission line ($T_{12}$). The gains of PID-controller are retuned employing (3) by the proposed QODSA method and at the end of optimization, controller gains are depicted in Table 3(a). The minimum ITAE value, settling time of $\Delta f$ and $\Delta P_{tie}$ with the said uncertainties is offered in Table 3 (a). Furthermore, the sensitivity of proposed controller for test system-1 is studied with the optimal controller values gained at the nominal operating condition as specified in Table 2 and static system performances, like fitness value and setting time of $\Delta f$ and $\Delta P_{tie}$ are displayed in Table 3(b). The dynamic responses of the concerned power system with the variations of $T_t$ and $T_{ps}$ are shown in Figs. 5 and 6. By the observation of Table 3(a) and (b) and Figs. 5 and 6, one can infer that there is an insignificant change in the system performance with the aforementioned variations and system performance is independent on the retuned gains of PID-controller. Thereby, controller parameters are need not be reset from their nominal setting for these variations.

In addition, to show the robustness of the designed controller, a sinusoidal load pattern as shown in Fig. 7(a) is applied to area-1 of test system-1 at $t = 0$ sec . Mathematically, the sinusoidal load pattern is defined in (13). The dynamic responses of the concerned power system in terms of changes of frequency and tie-line power are presented in Fig. 7(b) and (c). For better comparison, the output results obtained with DSA-tuned PID-controller is also shown in Fig. 7(b) and (c).

$$\Delta P_D = 0.03\sin(4.36t) + 0.05\sin(5.3t) - 0.1\sin(6t) \quad (13)$$

The output results demonstrate that the amplitude of $\Delta f$ and $\Delta P_{tie}$ oscillations are limited with designed QODSA-optimized PID-controller and show significant improvement in the system performance compare to DSA. However, the oscillations in $\Delta f$ and $\Delta P_{tie}$ are not damped out, since the sinusoidal load perturbation takes place simultaneously.

### 4.2. Test system-2

To demonstrate the usefulness of proposed QODSA, the study is forwarded to complex and realistic power system considering the effects of generation rate constraint (GRC) of steam turbine and governor dead band (GDB) nonlinearities. To show the ability of proposed method, three unequal all thermal power plant (area1: 2000 MW, area2: 4000 MW, area3: 8000 MW) with distinct

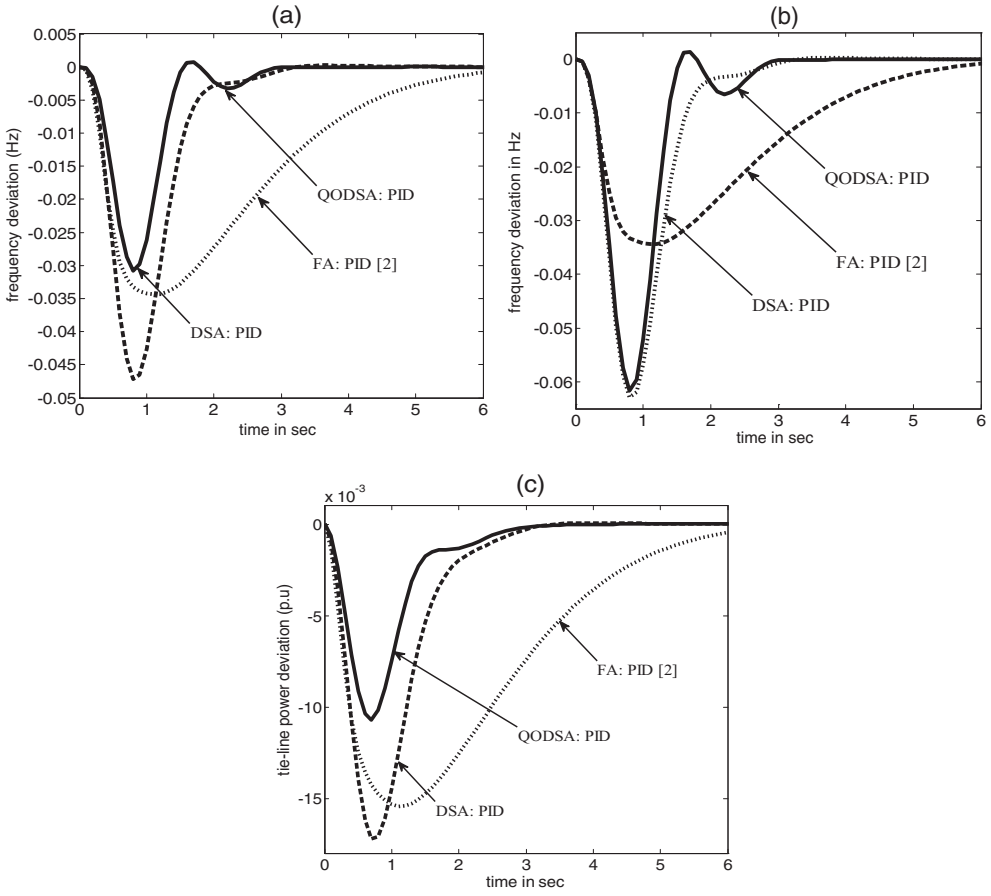


**Fig. 4.** Comparative transient responses of test system-1 after 10% SLP in area-1 with PID-controller, (a) change of frequency in area-1, (b) change of frequency in area-2, (c) change of tie-line power.

**Table 3(a)**
Sensitivity analysis with QODSA based PID-controller for test system-1.

| Parameter | % of change | Controller gains | | | | | | ITAE value | Settling time (sec) | | |
|---|---|---|---|---|---|---|---|---|---|---|---|
| | | $K_{i1}$ | $K_{i2}$ | $K_{p1}$ | $K_{p2}$ | $K_{d1}$ | $K_{d2}$ | | $\Delta f_1$ | $\Delta f_2$ | $\Delta P_{tie}$ |
| Nominal | No changes | 1.9524 | 0.0578 | 0.8246 | 1.9968 | 0.2630 | 0.4588 | 0.0664 | 1.72 | 2.75 | 2.92 |
| Loading condition | +50 | 1.9860 | 0.0079 | 0.9837 | 1.8307 | 0.3432 | 0.4587 | 0.1036 | 2.43 | 2.74 | 3.20 |
| | +25 | 1.9575 | 0.0215 | 1.0212 | 1.9733 | 0.3657 | 0.4779 | 0.0975 | 2.32 | 3.14 | 3.27 |
| | −25 | 1.9414 | 0.0034 | 1.0592 | 1.8497 | 0.4238 | 1.0579 | 0.0538 | 1.06 | 3.11 | 3.29 |
| | −50 | 1.9941 | −0.0103 | 0.9669 | 1.4862 | 0.3497 | 0.4641 | 0.0344 | 2.58 | 2.74 | 3.11 |
| $T_g$ | +50 | 1.9717 | 0.0039 | 1.0745 | 1.9654 | 0.4298 | 0.6928 | 0.0710 | 2.52 | 3.06 | 3.21 |
| | +25 | 1.9944 | −0.0002 | 1.0935 | 1.9856 | 0.4101 | 0.7365 | 0.0693 | 2.51 | 3.05 | 3.27 |
| | −25 | 1.9922 | −0.0049 | 0.9616 | 1.4058 | 0.3215 | 0.3515 | 0.0687 | 2.55 | 2.79 | 3.22 |
| | −50 | 1.9809 | 0.7926 | 1.0278 | 1.7605 | 0.3358 | 0.2949 | 0.0700 | 2.38 | 2.91 | 3.43 |
| $T_t$ | +50 | 1.9926 | 0.0123 | 1.4464 | 1.9337 | 0.5969 | 0.8738 | 0.0727 | 2.41 | 3.36 | 3.59 |
| | +25 | 1.9599 | −0.0006 | 0.6280 | 0.7394 | 0.2167 | 0.3322 | 0.0705 | 2.61 | 2.77 | 2.71 |
| | −25 | 1.9911 | 1.3016 | 0.8751 | 0.9687 | 0.3016 | 0.3601 | 0.0681 | 2.67 | 2.78 | 3.19 |
| | −50 | 1.9768 | −0.0012 | 0.6226 | 0.0173 | 0.1962 | 0.1504 | 0.0666 | 1.78 | 2.76 | 2.65 |
| $T_{ps}$ | +50 | 1.9938 | 0.0103 | 1.0268 | 1.9665 | 0.3388 | 0.6330 | 0.0774 | 2.11 | 3.25 | 3.12 |
| | +25 | 1.9659 | −0.0212 | 1.0289 | 1.4009 | 0.3748 | 0.5508 | 0.0731 | 2.84 | 2.98 | 3.00 |
| | −25 | 1.9033 | 0.0067 | 0.6164 | 1.1978 | 0.2565 | 0.4209 | 0.0714 | 2.57 | 2.45 | 2.68 |
| | −50 | 1.9088 | −0.0032 | 0.3762 | 1.0804 | 0.1879 | 0.4042 | 0.0697 | 2.47 | 2.15 | 2.39 |
| $T_{12}$ | +50 | 1.9802 | 0.3960 | 0.8443 | 1.9665 | 0.2768 | 0.6752 | 0.0574 | 1.41 | 2.36 | 2.47 |
| | +25 | 1.9730 | 0.0003 | 0.8711 | 1.7450 | 0.3054 | 0.5326 | 0.0627 | 2.36 | 2.48 | 2.62 |
| | −25 | 1.8557 | 0.0104 | 0.8428 | 0.9443 | 0.2946 | 0.3173 | 0.0889 | 3.04 | 3.16 | 3.51 |
| | −50 | 1.9095 | −0.0025 | 1.1480 | 0.5428 | 0.3519 | 0.1578 | 0.1094 | 3.35 | 4.77 | 4.91 |

controllers [2] is designed and dynamic responses of same are critically investigated. Linear transfer function model of test system-2 is displayed in Fig. 8 and nominal values of system parameters are available in Appendix. Initially, the linear model of test system 2 is developed and the classical controllers, i.e. I, PI, and PID, are separately designed with QODSA employing (3). The optimal controller settings, at the end of optimization, are specified in Table 4. The static system performance in terms of minimum fitness value and settling time of frequency and tie-line power deviations after 10% SLP in area-1 is also illustrated in Table 4. For better assessment of the controller performance, the dynamic behavior of test system 2 without any nonlinearity is depicted in Fig. 9 (a) and (b). It is clearly perceived from these figures that the dynamic behavior of concerned test system is remarkably improved

**Table 3(b)**
Sensitivity analysis of proposed controller with optimal gains obtained at nominal operating condition for test system-1.

| Parameter | % of change | ITAE value | Settling time (2% error band) | | | Parameter | % of change | ITAE value | Settling time (2% error band) | | | |
|---|---|---|---|---|---|---|---|---|---|---|---|---|
| | | | $\Delta f_1$ | $\Delta f_2$ | $\Delta P_{tie}$ | | | | $\Delta f_1$ | $\Delta f_2$ | $\Delta P_{tie}$ | |
| Loading condition | +50 | 0.1101 | 1.73 | 2.75 | 2.93 | $T_g$ | +50 | 0.0791 | 2.88 | 3.07 | 2.71 | |
| | +25 | 0.0917 | 1.73 | 2.75 | 2.92 | | +25 | 0.0795 | 2.16 | 2.68 | 2.86 | |
| | −25 | 0.0550 | 1.73 | 2.75 | 2.92 | | −25 | 0.0718 | 1.79 | 2.83 | 2.97 | |
| | −50 | 0.0367 | 1.73 | 2.76 | 2.93 | | −50 | 0.0717 | 1.87 | 2.93 | 3.01 | |
| $T_t$ | +50 | 0.0757 | 3.18 | 3.25 | 2.73 | $T_{ps}$ | +50 | 0.0789 | 2.86 | 3.41 | 3.16 | |
| | +25 | 0.0749 | 2.36 | 3.25 | 2.76 | | +25 | 0.0730 | 2.02 | 3.06 | 2.95 | |
| | −25 | 0.0700 | 1.71 | 2.95 | 3.075 | | −25 | 0.0693 | 2.46 | 2.81 | 3.05 | |
| | −50 | 0.0719 | 2.21 | 3.19 | 3.21 | | −50 | 0.0667 | 1.97 | 2.92 | 3.18 | |
| $T_{12}$ | +50 | 0.0651 | 2.13 | 3.11 | 2.93 | Nominal condition | No change | 0.0664 | 1.72 | 2.75 | 2.92 | |
| | +25 | 0.0660 | 1.56 | 2.48 | 2.58 | | | | | | | |
| | −25 | 0.0868 | 3.22 | 3.13 | 3.28 | Controller | $K_{i1}$ | $K_{i2}$ | $K_{p1}$ | $K_{p2}$ | $K_{d1}$ | $K_{d2}$ |
| | −50 | 0.1105 | 3.65 | 3.87 | 4.22 | Value | 1.9524 | 0.0578 | 0.8246 | 1.9968 | 0.2630 | 0.4588 |

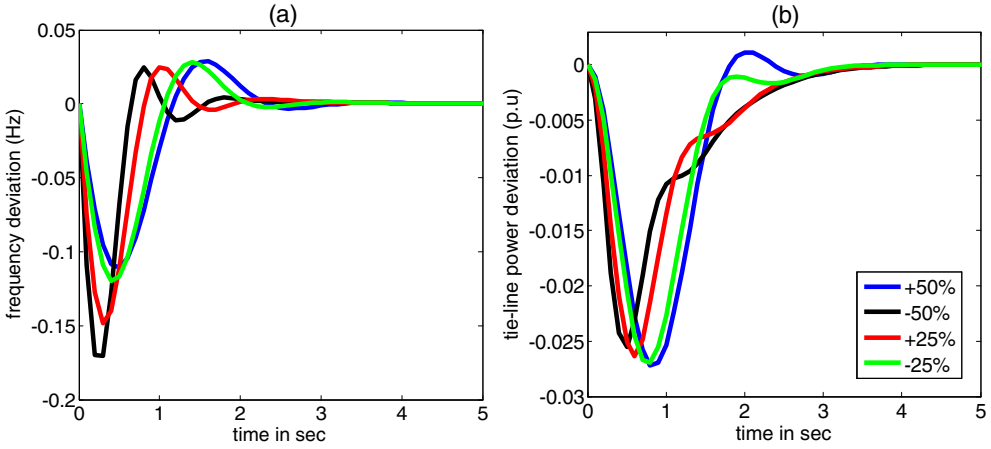


**Fig. 5.** Sensitivity analysis with QODSA-tuned PID-controller under the variation of $T_{ps}$ (a) change of frequency in area-1, (b) change of tie-line power.

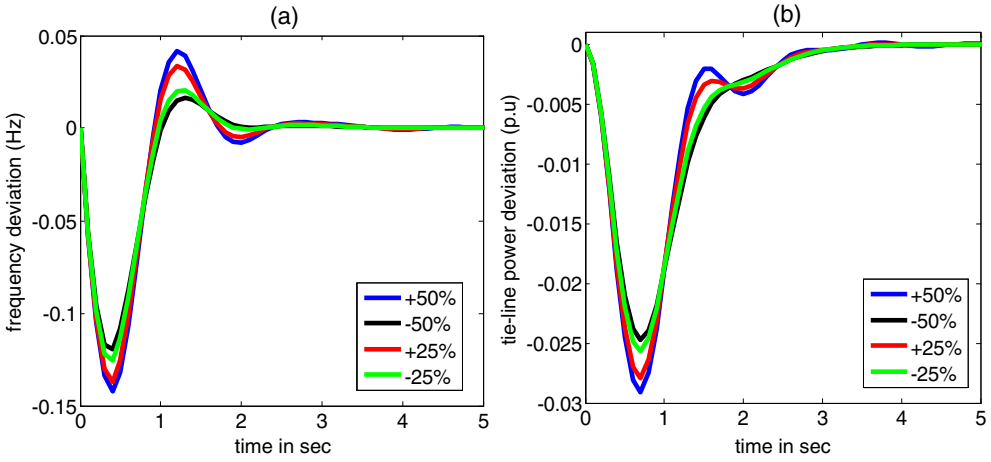


**Fig. 6.** Sensitivity analysis with QODSA-tuned PID-controller under the variation of $T_g$ (a) change of frequency in area-1, (b) change of tie-line power.

with PID-controller compared to PI and I-controllers. It is also noted from Fig. 9(a) and (b) that peak overshoot and undershoot of the transient responses are highly diminished with PID controllers.

For better assessment of the proposed algorithm and to get an accurate insight of power system dynamics, GRC and GDB nonlinearities are included in the system analysis. GRC is a common type of nonlinearity encountered in power system due to mechanical and thermodynamic constraints of the physical steam turbine. Practically GRC limits the power generation within the maximum specified value, if this constraint is not considered during the modeling of the power system, then the system may experience large momentary disturbances causing wear and tear of the controllers. A GRC of 3%/min is considered for the present study. GDB is another common type of nonlinearity faced in the power system. It is defined as the total magnitude of sustained speed changes within which there is no resulting change in valve positions [41]. The limiting value of GDB is specified to 0.06% for the large steam turbine [41].

The optimum values of controller's gains, minimum fitness values, and settling time (2% error band) of frequency and tie-line power flow with QODSA including GRC and GDB are illustrated

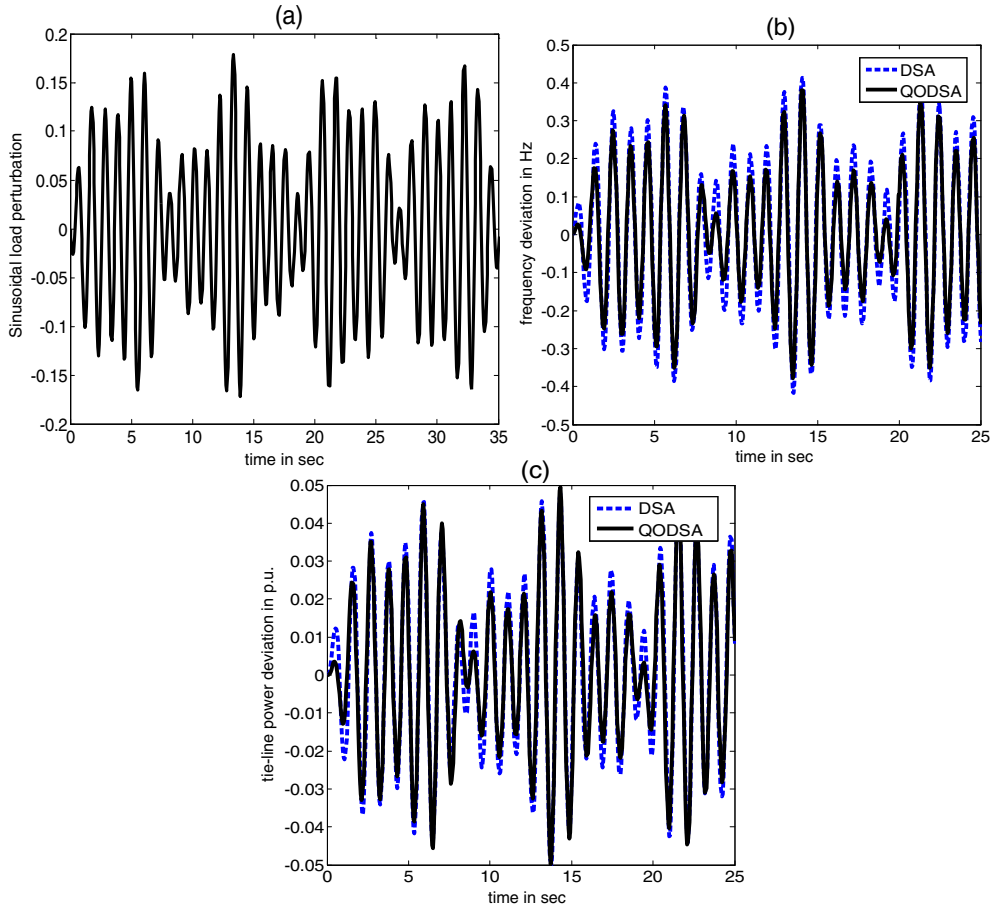


**Fig. 7.** (a) Random Sinusoidal load pattern, (b) change of frequency, (c) change of tie-line power, with QODSA based PID-controller.

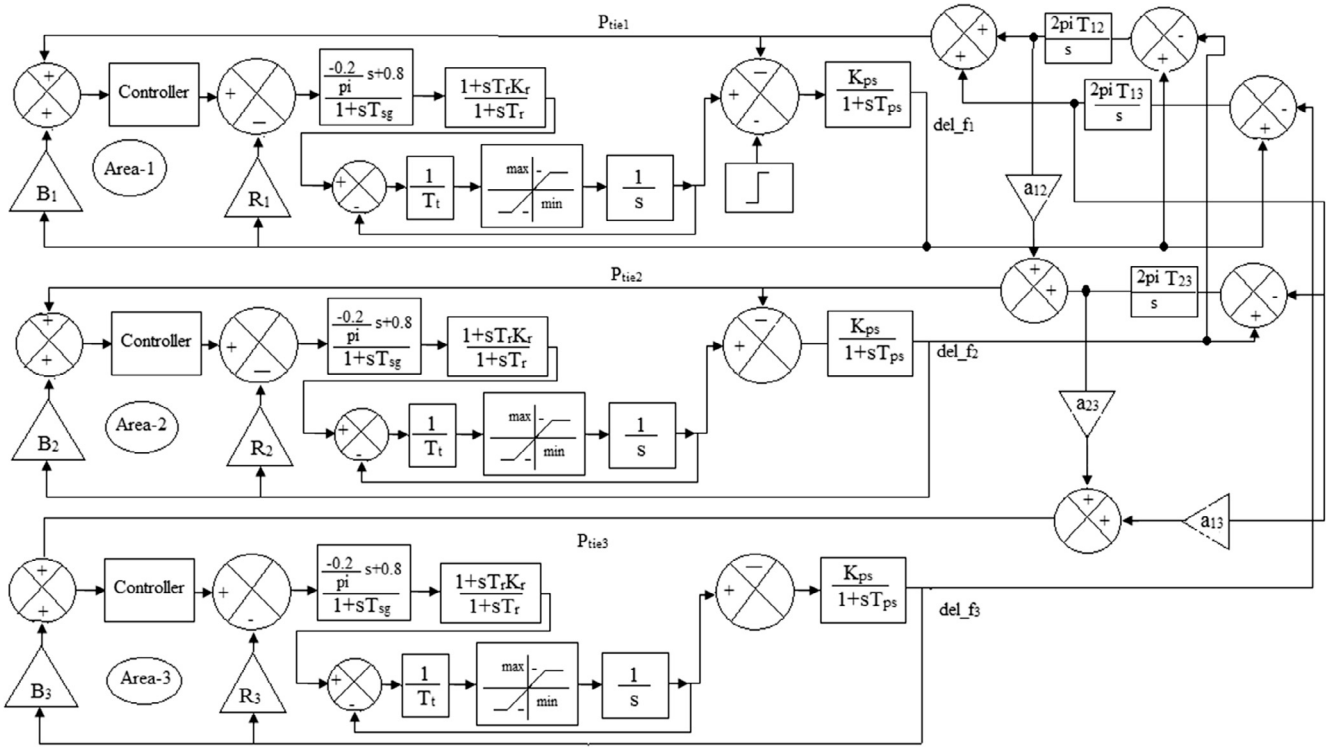


**Fig. 8.** Block diagram of three-unequal-all-thermal power plant with GRC and GDB nonlinearities [2].

**Table 4**
Optimum value of controller settings and fitness value of test system-2 after 10% SLP in area-1.

| Linear system (without GRC and GDB) | | | | | | | | | | | | | | | | |
|---|---|---|---|---|---|---|---|---|---|---|---|---|---|---|---|---|
| Optimization algorithm | Controller gains | | | | | | | | | ITAE value | Settling time (2% error band) | | | | | |
| | $K_{i1}$ | $K_{i2}$ | $K_{i3}$ | $K_{p1}$ | $K_{p2}$ | $K_{p3}$ | $K_{d1}$ | $K_{d2}$ | $K_{d3}$ | | $\Delta f_1$ | $\Delta f_2$ | $\Delta f_3$ | $\Delta P_{tie1}$ | $\Delta P_{tie2}$ | $\Delta P_{tie3}$ |
| QODSA: I | 0.4479 | 0.0105 | 0.4697 | – | – | – | – | – | – | 2.1902 | 17.20 | 19.93 | 16.63 | 21.82 | 21.43 | 23.92 |
| QODSA: PI | 0.9986 | −0.0048 | 0.4651 | −0.8080 | 0.4936 | 1.7308 | – | – | – | 0.9096 | 6.65 | 9.60 | 9.59 | 11.02 | 9.05 | 11.78 |
| QODSA: PID | 1.8695 | 1.6810 | 1.8256 | 1.9754 | 1.9426 | 1.9876 | 0.7948 | 0.7942 | 0.6350 | **0.2197** | 5.98 | 10.16 | 11.82 | 14.69 | 13.29 | 15.22 |
| Non-linear System (with GRC and GDB) | | | | | | | | | | | | | | | | |
| Optimization algorithm | Controller gains | | | | | | | | | ITAE value | Settling time (2% error band) | | | | | |
| | $K_{i1}$ | $K_{i2}$ | $K_{i3}$ | $K_{p1}$ | $K_{p2}$ | $K_{p3}$ | $K_{d1}$ | $K_{d2}$ | $K_{d3}$ | | $\Delta f_1$ | $\Delta f_2$ | $\Delta f_3$ | $\Delta P_{tie1}$ | $\Delta P_{tie2}$ | $\Delta P_{tie3}$ |
| GA: I [2] | −0.9303 | −0.9033 | −1.001 | – | – | – | – | – | – | 139.93 | 98.01 | 78.21 | 79.59 | 99.98 | 54.65 | 73.78 |
| FA: I [2] | −0.8952 | −0.3801 | −0.1204 | – | – | – | – | – | – | 124.98 | 94.00 | 71.32 | 72.68 | 96.90 | 48.50 | 66.91 |
| FA: PI [2] | −0.7821 | −0.5390 | 0.0042 | 0.5427 | 0.0487 | −0.0381 | – | – | – | 46.51 | 32.37 | 31.59 | 31.47 | 33.29 | 26.48 | 25.78 |
| FA: PID [2] | −1.6021 | −0.2000 | −0.1257 | −1.5293 | −1.6612 | −0.1738 | −1.1051 | −1.3578 | −0.2705 | 30.9 | 26.56 | 26.72 | 26.55 | 24.03 | 19.66 | 20.70 |
| QODSA: I | 0.4484 | −0.0178 | 0.6677 | – | – | – | – | – | – | 2.7039 | 17.77 | 17.39 | 16.64 | 22.7 | 30.6 | 29.9 |
| QODSA: PI | 1.3739 | 0.1107 | −0.2160 | −0.9016 | 0.1719 | 1.1098 | – | – | – | 1.5494 | 26.29 | 27.12 | 23.14 | 33.18 | 29.01 | 38.13 |
| QODSA: PID | 1.8830 | 1.2259 | 1.3832 | 1.9812 | 1.5761 | 0.8575 | 0.9198 | 0.7698 | 0.7566 | **0.2250** | 18.61 | 20.60 | 24.42 | 23.47 | 19.59 | 18.74 |

Bold faces show the best value.

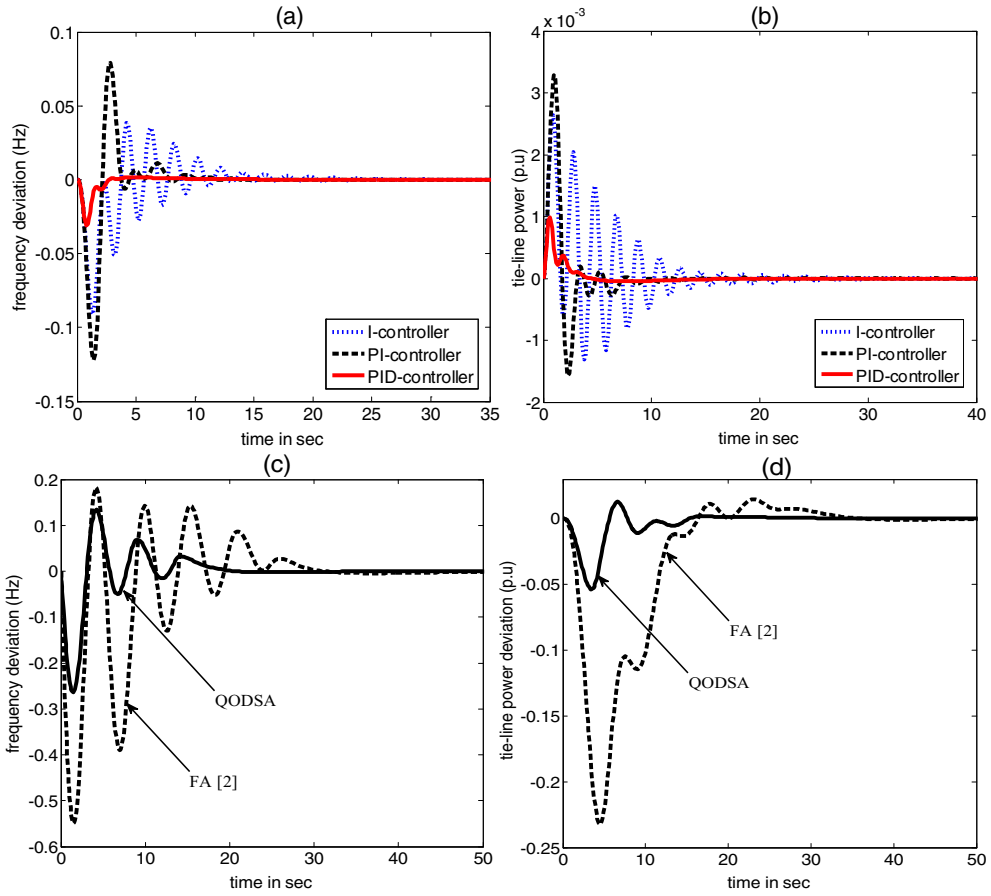


**Fig. 9.** Comparative transient responses of test system-2 after 10% SLP in area-1 (a) change of frequency in area-1, (b) change of tie-line power, (c) change of frequency in area-1 including GRC and GDB, (d) change of tie-line power including GRC and GDB.

in Table 4. An extensive comparative analysis has been performed to show the superiority of proposed QODSA over FA [2], GA [2] for the similar test system. For comparison, the results obtained with GA and FA for similar test system is also presented in Table 4. It is evident from Table 4 that minimum fitness value (ITAE = 0.2250) is obtained with QODSA: PID compared to FA (ITAE = 30.9) and the improvement of ITAE value is 99.27%. It is further noted from Table 4 that settling time of frequency and tie-line power oscillations is minimized with QODSA and improvement of same is 29.93% ($\Delta P_{tie,2}$), 22.9% ($\Delta f_3$), 8.02%($\Delta f_3$), 2.33%($\Delta P_{tie,1}$), 0.35% ($\Delta P_{tie,2}$), and 9.47% ($\Delta P_{tie,3}$) compared to FA. The signals of the closed loop system are displayed in Fig. 9(c) and (d). It is clearly viewed from Fig. 9(c) and (d) that QODSA based PID-controller gives better transient performances than that obtained with FA based PID controller in terms of overshoot, undershoot, and settling time. Simulation results verify that proposed method is superior to damp out the system oscillations caused by SLP. Hence, it may be concluded from the aforesaid discussion that the

proposed method assured system stability in the presence of nonlinearities and provides improved results compared to other existing control algorithms.

*4.2.1. Robustness analysis of test system-2*

To study the robustness of the designed controller, RLP as shown in Fig. 10(a) is applied to area-1 of test system-2. The system dynamics after the load perturbation is shown in Fig. 10 (b) and (c). It is clearly viewed from Fig. 10(b) and (c) that oscillation in frequency and tie-line power is effectively die out and change of amplitude with this RLP is within the tolerable limit, and hence robustness of the designed controllers is validated.

Further to investigate the superiority of the proposed method, simultaneous step load increase of 10% in area-1 and separately 5% and 10% SLP in area-2 are applied to test system-2. The system dynamics under this scenario are presented in Fig. 11. It is viewed from Fig. 11 that with this simultaneous load perturbation, number of oscillations and settling time of frequency and tie-line power oscillations are increased. Critical review of presented results shows that the power system does not lost the system stability under this serious perturbed condition. It may also be pointed that QODSA-tuned PID-controllers are robust and performed satisfactorily with the application of multiple load disturbances.

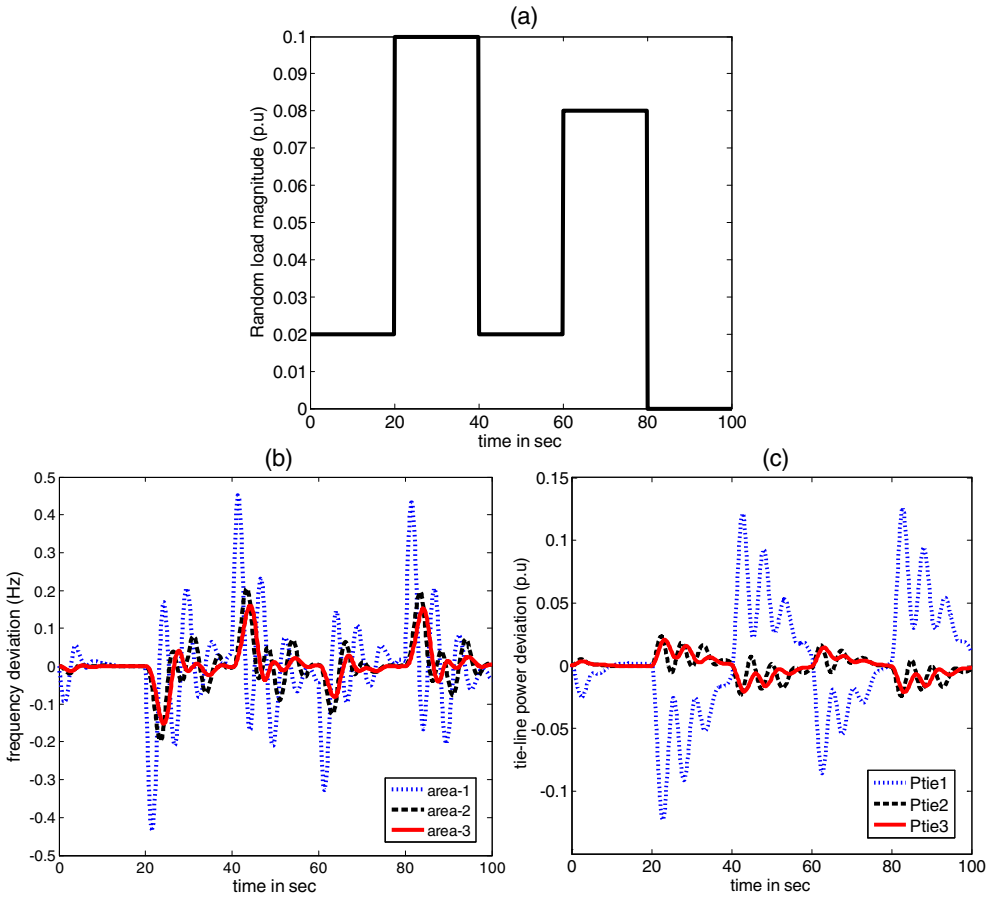


**Fig. 10.** (a) random load pattern, (b) Change of frequency, (c) change of tie-line power of test system-2 including GRC and GDB effect.

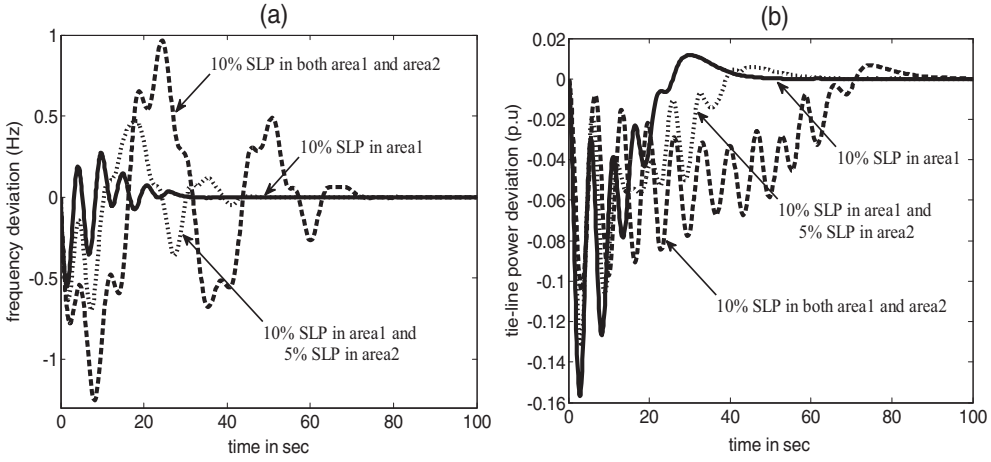


**Fig. 11.** (a) Changes of frequency, (b) changes of tie-line power, under different loading condition for test system-2 including GRC and GDB.

### 4.3. Test system-3

#### 4.3.1. Without nonlinearities

To examine the effectiveness of proposed algorithm, the study if further extended to another complex and realistic interconnected power system network. Two-area multi-unit multi-source power plant equipped with PI/PID controller is taken from [35] and its dynamic responses after 1% SLP in area-1 is investigated. The linear transfer function model of the concerned power system is shown in Fig. 12 [35] and nominal system parameters are appended in Appendix. Initially, QODSA is employed to search the optimum settings of PI/PID controller using (3) and then the effect of GRC on the system dynamics has been investigated. The optimum controller settings and system performances in terms of ITAE value, settling time of frequency and tie-line power deviations are given in Table 5. The dynamic behavior of concerned power system with QODSA-tuned PI/PID controller excluding nonlinearity is depicted in Fig. 13. It is clearly viewed from Fig. 13 that QODSA-tuned PID-controller improved system performances remarkably than that of QODSA-tuned PI-controller. To show the superiority of proposed QODSA, the output results are compared with some recently published control algorithms, which are enumerated in Table 6. A critical investigation of Table 6 reveals that proposed QODSA-optimized PID gives minimum fitness value compared to others. Hence, it may be concluded from Tables 5 and 6 that QODSA based PID controller outperforms other.

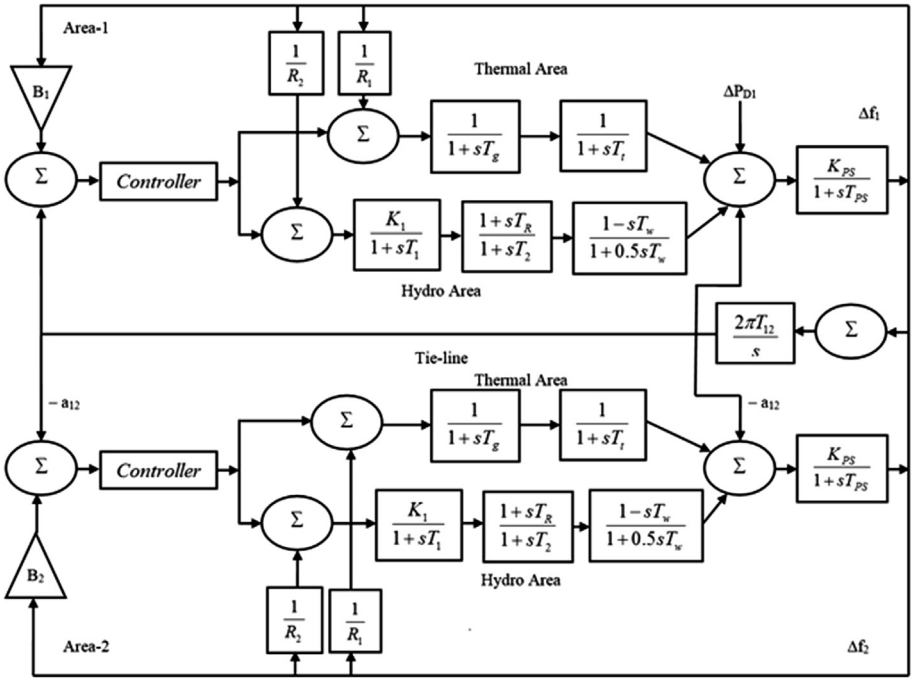


**Fig. 12.** Transfer function model of two-area multi-unit mult-source hydro-thermal power plant [37].

**Table 5**
Optimum values of controller parameters and system performances of test system-3 after including GRC.

| Linear system | | | | | | | | | | | | |
|---|---|---|---|---|---|---|---|---|---|---|---|---|
| Types of Controller | Area-1 | | | | | | Area-2 | | | | | |
| | $K_{p1}$ | $K_{i1}$ | $K_{d1}$ | $K_{p2}$ | $K_{i2}$ | $K_{d2}$ | $K_{p3}$ | $K_{i3}$ | $K_{d3}$ | $K_{p4}$ | $K_{i4}$ | $K_{d4}$ |
| PI | 0.1317 | 0.8824 | – | 0.0723 | 0.0113 | – | 1.1696 | 0.2755 | – | 0.0400 | 1.6843 | – |
| PID | 1.1151 | 1.8550 | 0.6207 | 1.8996 | 0.0859 | 1.1117 | 1.9322 | 0.4534 | 0.6498 | 1.3186 | 0.0277 | 1.4731 |
| Settlingtime: PI controller | $\Delta f_1$ | 7.53 | Fitness value | ITAE | 0.0571 | Settlingtime: PID controller | $\Delta f_1$ | 1.13 | Fitness value | ITAE | 0.0109 | |
| | $\Delta f_2$ | 9.93 | | ISE | $1.1371 \times 10^{-4}$ | | $\Delta f_2$ | 4.34 | | ISE | $1.4969 \times 10^{-5}$ | |
| | $\Delta P_{tie}$ | 8.66 | | ITSE | $1.5069 \times 10^{-4}$ | | $\Delta P_{tie}$ | 4.51 | | ITSE | $1.4952 \times 10^{-5}$ | |

| Nonlinear system (with GRC only) | | | | | | | | | | | | |
|---|---|---|---|---|---|---|---|---|---|---|---|---|
| Controller gains | Area-1 | | | | | | Area-2 | | | | | |
| | $K_{p1}$ | $K_{i1}$ | $K_{d1}$ | $K_{p2}$ | $K_{i2}$ | $K_{d2}$ | $K_{p3}$ | $K_{i3}$ | $K_{d3}$ | $K_{p4}$ | $K_{i4}$ | $K_{d4}$ |
| Optimum values | 1.9207 | 1.9880 | 0.4013 | 0.8042 | 0.3431 | 0.7294 | 1.6925 | 1.9874 | 0.4733 | 0.8042 | 0.7689 | 0.7395 |
| Frequency stabilizer | $K_{SMES\_1}$ | $T_{SMES\_1}$ | $T_{11}$ | $T_{12}$ | $T_{13}$ | $T_{14}$ | $K_{SMES\_2}$ | $T_{SMES\_2}$ | $T_{21}$ | $T_{22}$ | $T_{23}$ | $T_{24}$ |
| Optimum values | 0.9960 | 0.1131 | 0.5659 | 0.5283 | 0.9669 | 0.6981 | 0.2073 | 0.6160 | 0.6363 | 0.9884 | 0.6231 | 0.0550 |
| Transient specifications | Overshoot ($\times 10^{-4}$) | | | Undershoot (−ve) | | | Settling time (2% error band) | | | ISE value ($\times 10^{-7}$) | ITAE value | ITSE value ($\times 10^{-7}$) |
| | $\Delta f_1$ | $\Delta f_2$ | $\Delta P_{tie}$ | $\Delta f_1$ | $\Delta f_2$ | $\Delta P_{tie}$ | $\Delta f_1$ | $\Delta f_2$ | $\Delta P_{tie}$ | | | |
| | 1.51 | 1.49 | 0.258 | 0.0162 | 0.0172 | 0.0032 | 10.91 | 12.39 | 13.56 | 1.2202 | 0.0369 | 9.4075 |

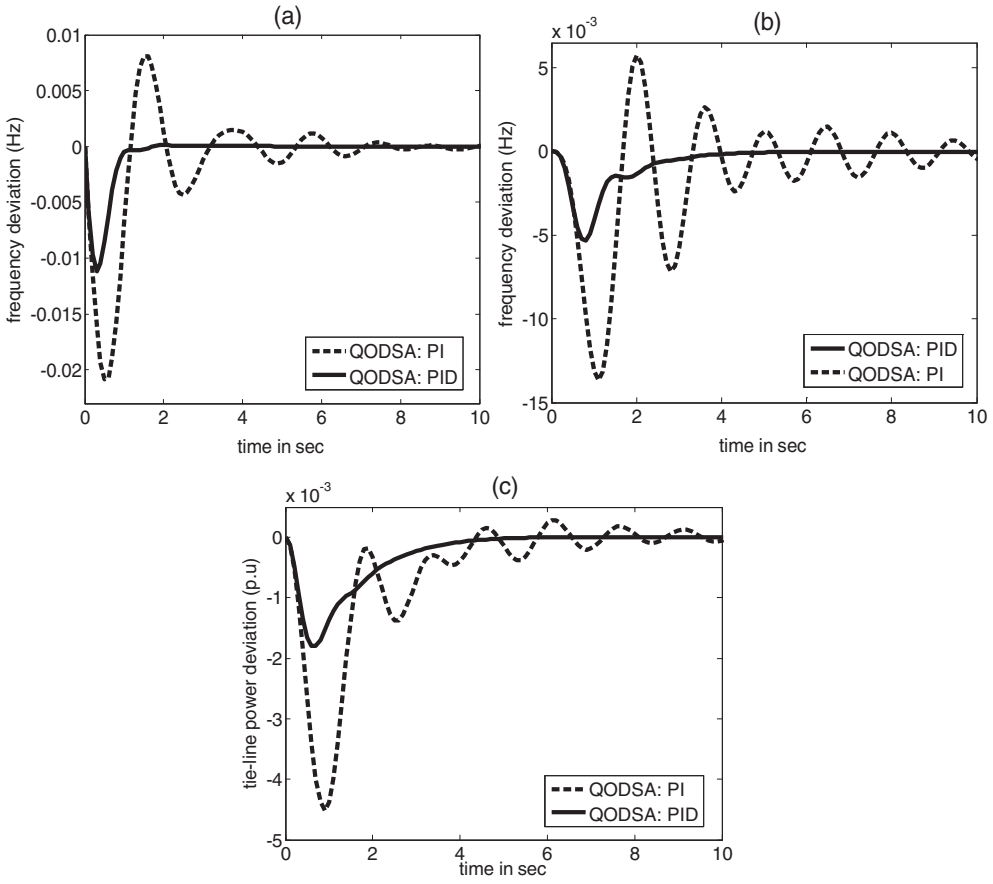


**Fig. 13.** Transient behavior of test system-3 after 1% SLP in area-1 without nonlinearity, (a) frequency deviation in area-1, (b) frequency deviation in area-2, (c) tie-line power deviation.

**Table 6**
Comparison between various controllers in terms of performance indices.

| Proposed controllers | | Performance indices | | |
|---|---|---|---|---|
| | | ISE ($\times 10^{-4}$) | ITAE | ITSE ($\times 10^{-4}$) |
| Proposed EA | QODSA based PI controller | 1.1371 | 0.0571 | 1.5069 |
| | QODSA based PID controller | **0.14969** | **0.0109** | **0.14952** |
| [35] | ZN based PI controller | 10.79 | 1.336 | 28.9 |
| | VSS based ZN tuned PI Controller | 9.564 | 0.8793 | 14.8 |
| | GA based PI controller | 9.058 | 0.6253 | 12.38 |
| | VSS based GA tuned PI controller | 8.815 | 0.6243 | 11.95 |
| | Fuzzy gain scheduling | 1.63 | 0.1868 | 1.553 |
| | Variable structure based FGS | 1.545 | 0.1856 | 1.517 |

Bold signifies best results.

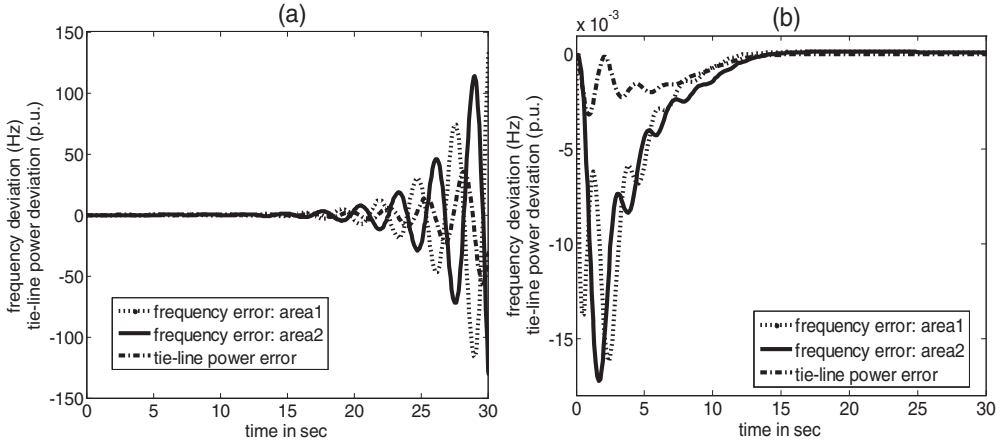


**Fig. 14.** Transient responses of test system-3 after 1% SLP in area-1 including GRC, (a) without frequency stabilizer, (b) with frequency stabilizer.

*4.3.2. With nonlinearities and SMES controller*

Furthermore, to demonstrate the ability of the proposed algorithm, the appropriate value of GRC is considered during the simulation and system dynamics with GRC subjected to load perturbation is shown in Fig. 14(a). It is clearly observed from Fig. 14(a) that the system approaches to the instability as time progresses, which is further verified from the Eigen value analysis of the same (it is not given in this article). To retrieve the system stability, authors have proposed an optimal frequency stabilizer in the form of superconducting magnetic energy storage (SMES) in coordination with PID-controller. The optimum settings of coordinated controllers are illustrated in Table 5. The system dynamics with

**Table 7**
Optimum values of coordinated controller and transient specifications of test system-3 with nonlinearities.

| Nonlinear system (with GRC, GDB and boiler dynamics): DSA | | | | | | | | | | | | |
|---|---|---|---|---|---|---|---|---|---|---|---|---|
| Controller gains | Area-1 | | | | | | Area-2 | | | | | |
| | $K_{p1}$ | $K_{i1}$ | $K_{d1}$ | $K_{p2}$ | $K_{i2}$ | $K_{d2}$ | $K_{p3}$ | $K_{i3}$ | $K_{d3}$ | $K_{p4}$ | $K_{i4}$ | $K_{d4}$ |
| Optimum values | 1.2049 | 1.7681 | 0.6927 | 1.7026 | 0.3292 | 0.5252 | 0.4243 | 0.5419 | 1.1973 | 0.2925 | 1.7176 | 1.0223 |
| Frequency stabilizer | $K_{SMES\_1}$ | $T_{SMES\_1}$ | $T_{11}$ | $T_{12}$ | $T_{13}$ | $T_{14}$ | $K_{SMES\_2}$ | $T_{SMES\_2}$ | $T_{21}$ | $T_{22}$ | $T_{23}$ | $T_{24}$ |
| Optimum values | 0.9815 | 0.2710 | 0.9845 | 0.3010 | 0.9679 | 0.5507 | 0.3657 | 0.6222 | 0.2870 | 0.6504 | 0.5757 | 0.4618 |
| Transient specifications | Overshoot ($\times 10^{-4}$) | | | Undershoot (−ve) | | | Settling time (2% error band) | | | ISE value ($\times 10^{-7}$) | ITAE value | ITSE value ($\times 0^{-7}$) |
| | $\Delta f_1$ | $\Delta f_2$ | $\Delta P_{tie}$ | $\Delta f_1$ | $\Delta f_2$ | $\Delta P_{tie}$ | $\Delta f_1$ | $\Delta f_2$ | $\Delta P_{tie}$ | | | |
| | 3.47 | 2.17 | 0.267 | 0.0163 | 0.0151 | 0.0036 | 15.9 | 13.09 | 19.05 | 3.16 | 0.0508 | 1.73 |
| Nonlinear system (with GRC, GDB and boiler dynamics): QODSA | | | | | | | | | | | | |
| Controller gains | Area-1 | | | | | | | | Area-2 | | | |
| | $K_{p1}$ | $K_{i1}$ | $K_{d1}$ | $K_{p2}$ | $K_{i2}$ | $K_{d2}$ | $K_{p3}$ | $K_{i3}$ | $K_{d3}$ | $K_{p4}$ | $K_{i4}$ | $K_{d4}$ |
| Optimum values | 1.0927 | 1.9738 | 0.8398 | 1.4485 | 0.2071 | 1.0908 | 1.5798 | 0.1351 | 1.5324 | 1.5294 | 1.5739 | 1.2056 |
| Frequency stabilizer | | $T_{SMES\_1}$ | $T_{11}$ | $T_{12}$ | $T_{13}$ | $T_{14}$ | $K_{SMES\_2}$ | $T_{SMES\_2}$ | $T_{21}$ | $T_{22}$ | $T_{23}$ | $T_{24}$ |
| Optimum values | 0.9355 | 0.4045 | 0.8702 | 0.2915 | 0.6880 | 0.7149 | 0.9711 | 0.3673 | 0.7642 | 0.9406 | 0.3950 | 0.0958 |
| Transient specifications | Overshoot ($\times 10^{-4}$) | | | Undershoot (−ve) | | | Settling time (2% error band) | | | ISE value ($\times 10^{-7}$) | ITAE value | ITSE value ($\times 10^{-7}$) |
| | $\Delta f_1$ | $\Delta f_2$ | $\Delta P_{tie}$ | $\Delta f_1$ | $\Delta f_2$ | $\Delta P_{tie}$ | $\Delta f_1$ | $\Delta f_2$ | $\Delta P_{tie}$ | | | |
| | 3.25 | 3 | 0.227 | 0.0168 | 0.0151 | 0.0036 | 11.63 | 11.49 | 18.2 | 2.48 | 0.0399 | 1.52 |

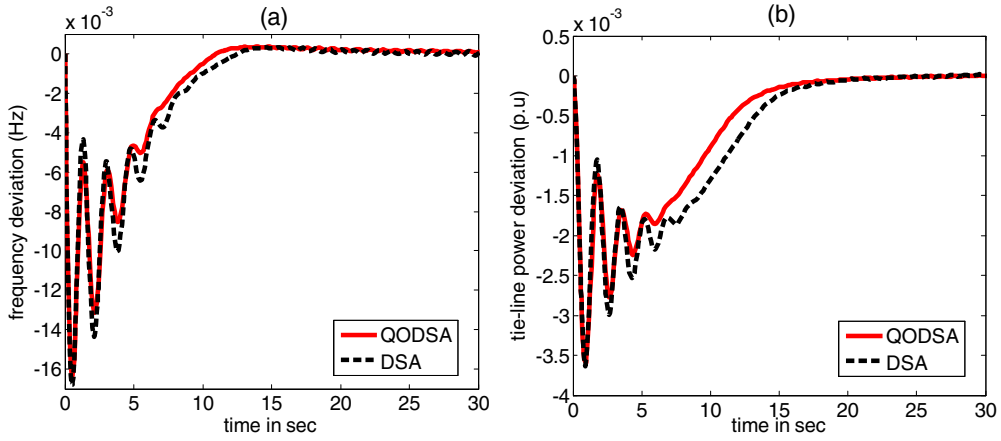


**Fig. 15.** Transient responses of test system-3 after 1% SLP in area-1 including GRC, GDB, and BD, (a) change of frequency in area-1, (b) changes of tie-line power.

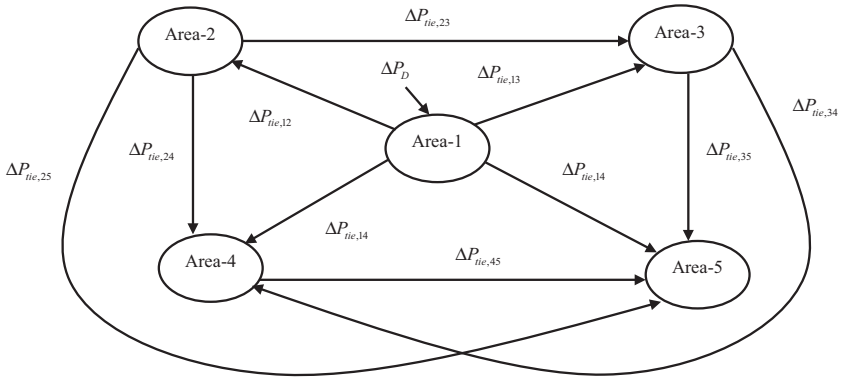


**Fig. 16.** Schematic diagram of five-area thermal power plant.

coordinated PID-SMES controller is shown in Fig. 14(b) and settling times of frequency and tie-line power deviation are presented in Table 5. It is remarkable from Fig. 14(b) that the proposed optimum coordinated controller retrieves the system stability and gives acceptable performance under the disturbed condition.

To ascertain the preeminence and success of proposed QODSA method to cope with nonlinear LFC system, the test system-3 is further studied with two more nonlinearities of power system namely "boiler dynamics" and "governor dead band". The boiler is a device meant for producing steam under pressure. The block diagram of drum type boiler is available in [42], which involves a large time delay in the fuel system. Pade approximation and signal flow graph (SFG) methods are used to linearize this nonlinearity for investigating its effect on the system dynamics. For a linearized model of time-delay terms (fuel system), readers are referred to [42]. Proposed QODSA is employed to tune the coordinated PID-SMES controller gains via the minimization of ITAE based fitness function considering the aforesaid nonlinearities. The same procedure as presented in Section 3.3 is followed to tune the PID-SMES coordinated controller. 1% SLP is given to area-1 for identifying the dynamic stability of the concerned power system. The optimal controller gains, minimum fitness value, and settling time of frequency and tie-line power oscillations are depicted in Table 7. To affirm the superiority of proposed QODSA technique, the system performances with DSA-tuned coordinated PID-SMES controller is also presented in Table 7. It is remarkable that lower the fitness value,

**Table 8**
Optimal controller gains for test system-4 with DSA and QODSA.

| Control algorithms | | Area-1 | Area-2 | Area-3 | Area-4 | Area-5 | Fitness value |
|---|---|---|---|---|---|---|---|
| DSA: PID | $k_p$ | 0.7962 | 0.5830 | 0.1335 | 0.1929 | 0.8975 | $1.3610 \times 10^{-4}$ |
| | $k_i$ | 0.9772 | 0.9496 | 0.7871 | 0.1049 | 0.4966 | |
| | $k_d$ | 0.1881 | 0.9641 | 0.7898 | 0.0891 | 0.8042 | |
| | Peak overshoot | **0.0089** | 0.0205 | **0.0075** | $\mathbf{1.49 \times 10^{-4}}$ | **0.0059** | |
| | Settling time (in sec) | 18.66 | 16.74 | 18.45 | 19.05 | 21.04 | |
| QODSA: PID | $k_p$ | 0.9656 | 0.8109 | 0.8091 | 0.8022 | 0.3590 | $\mathbf{9.8416 \times 10^{-5}}$ |
| | $k_i$ | 0.7055 | 0.2189 | 0.6700 | 0.9293 | 0.5856 | |
| | $k_d$ | 0.9518 | 0.2669 | 0.4031 | 0.4269 | 0.3626 | |
| | Peak overshoot | 0.0198 | $\mathbf{7.50 \times 10^{-4}}$ | 0.0287 | 0.0121 | 0.0128 | |
| | Settling time (in sec) | **16.32** | **13.82** | **17.94** | **17.41** | **17.61** | |

Bold face show the best results.

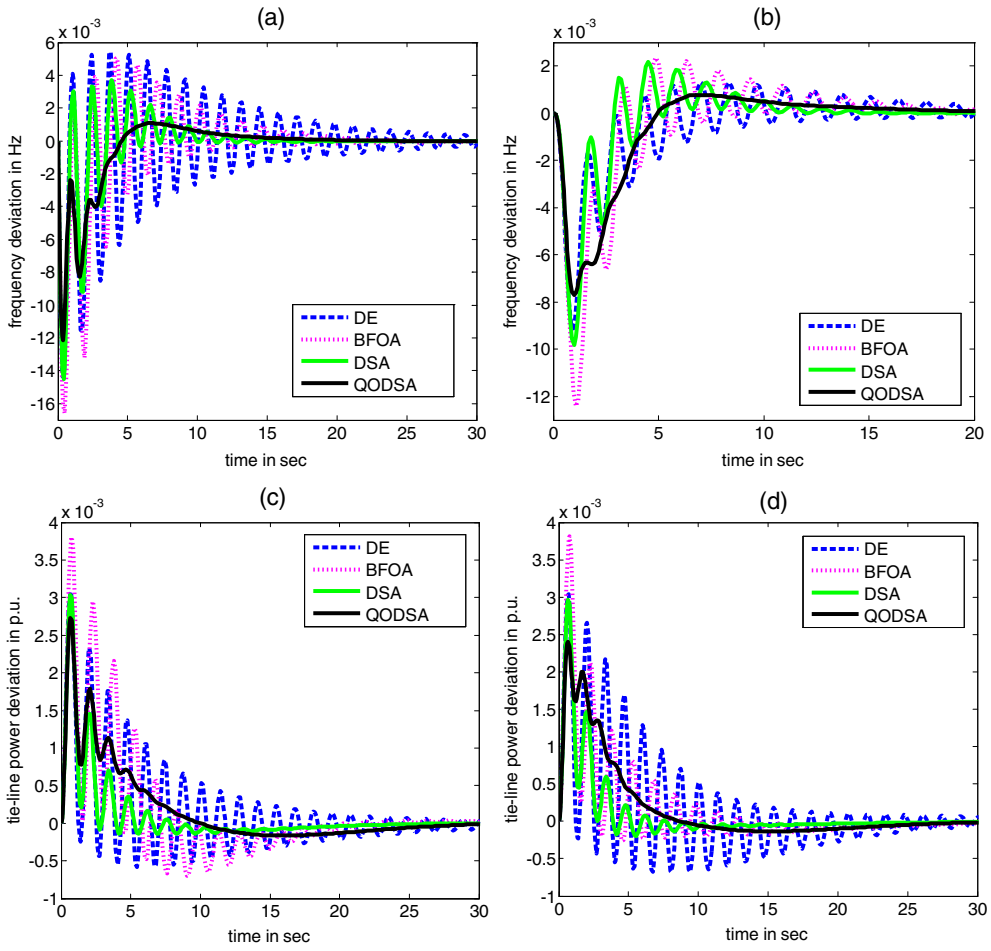


**Fig. 17.** Dynamic performance of test system-4 with GRC, (a) change of frequency in area-1, (b) change of frequency in area-3, (c) change of tie-line power $\Delta P_{tie,23}$, (d) change of tie-line power $\Delta P_{tie,45}$.

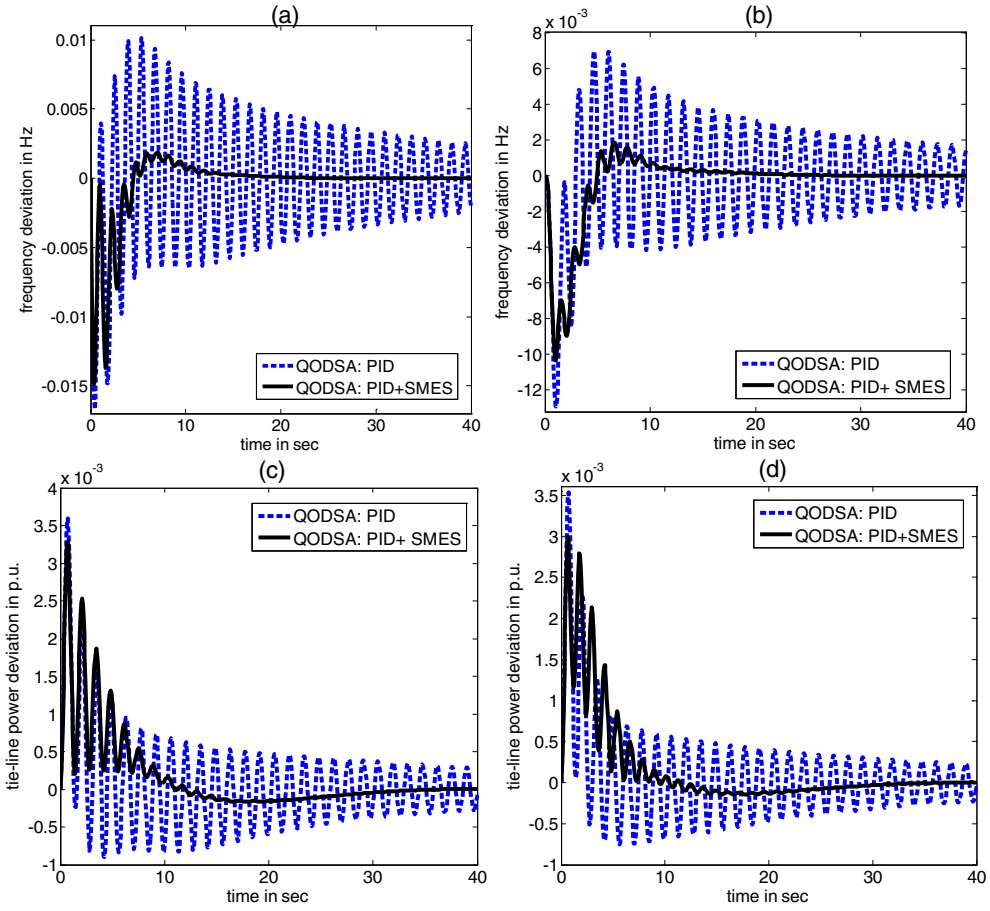


**Fig. 18.** Dynamic performance of test system-4 with GRC and GDB, (a) change of frequency in area-1, (b) change of frequency in area-3, (c) change of tie-line power $\Delta P_{tie,23}$, (d) change of tie-line power $\Delta P_{tie,45}$.

better the system responses in terms of time domain specifications. It is evident from Table 7 that the fitness value is further minimized with coordinated controllers and improvement of same is **21.45%**. The dynamic responses of concerned power system with said nonlinearities are displayed in Fig. 15. Improvements of 26.86% ($\Delta f_1$), 12.22% ($\Delta f_2$), and 4.46% ($\Delta P_{tie}$), are also noted for settling time with the utilization of QODSA-based coordinated PID-SMES controller. From Fig. 15 and Table 7 it is observed that proposed algorithm yields better dynamic response compared to DSA. It may also be noted that oscillations are highly attenuated and the system gives a higher degree of stability in the presence of said nonlinearities.

### 4.4. Test system-4

#### 4.4.1. With PID-controllers and GRC

To demonstrate the tuning ability of QODSA to cope up with large interconnected power system with distinct controllers, one more test system namely five-area thermal power plant is designed and analyzed. The investigated system comprises of a five-area unequal thermal power plant of area-1: 2000 MW, area-2: 4000 MW, area-3: 8000 MW, area-4: 10,000 MW, and area-5: 12,000 MW [36]. The schematic diagram of test system is shown in Fig. 16, however, the linear approximated model of same is available in [36]. The PID-controllers are employed in each control area and its gains are optimally searched by the QODSA. In this phase of a simulation study, ISE based fitness function is considered to design the PID-controllers as specified in [36] and the controller gains are set between (0, 1). The selected objective function is defined in (14). A step load increase of 0.01 *p.u.* at $t = 0$ sec is considered to assess the dynamic performance of concerned power system. To add some degree of nonlinearity, GRC of 3%/min in each area is included in the simulation study.

$$J_{ISE} = \int_0^T (ACE_i)^2 dt \qquad i = 1,2,3,4,5 \tag{14}$$

The optimal PID-controller gains with original DSA and QODSA are presented in Table 8. Minimum fitness value computed with QODSA-tuned PID-controller is **ISE = 9.8416 × 10$^{-5}$**, which is further minimized by **27.69%** compared to original DSA. The comparative convergence characteristic of DSA and QODSA for the concerned test system is shown in Fig. 2(c). It is remarkable from Fig. 2(c) that fitness value decreases with generation and approaches to the optimal solution within iterations. Moreover, QODSA converges at a faster rate than DSA.

To show the advantage, the results obtained by the QODSA are compared to that of original DSA, BFOA, and DE algorithms. However, the controller gains computed by the BFOA and DE algorithms are not shown in this article. The dynamic performance of the concerned power system subjected to SLP in area-1 is shown in Fig. 17 (a)–(d). The settling time and peak overshoot of frequency and tie-line power deviations are noted from Fig. 17(a)–(d) and offered in Table 8. For better comparison, the dynamic behavior of test system-4 with DSA, BFOA, and DE are also shown in Fig. 17(a)–(d). A critical review of Fig. 17(a)–(d) reveals that proposed QODSA-tuned PID-controllers provide better outputs than that obtained by DSA, BFOA, and DE algorithms. Only four figures are shown for justifying the above statements.

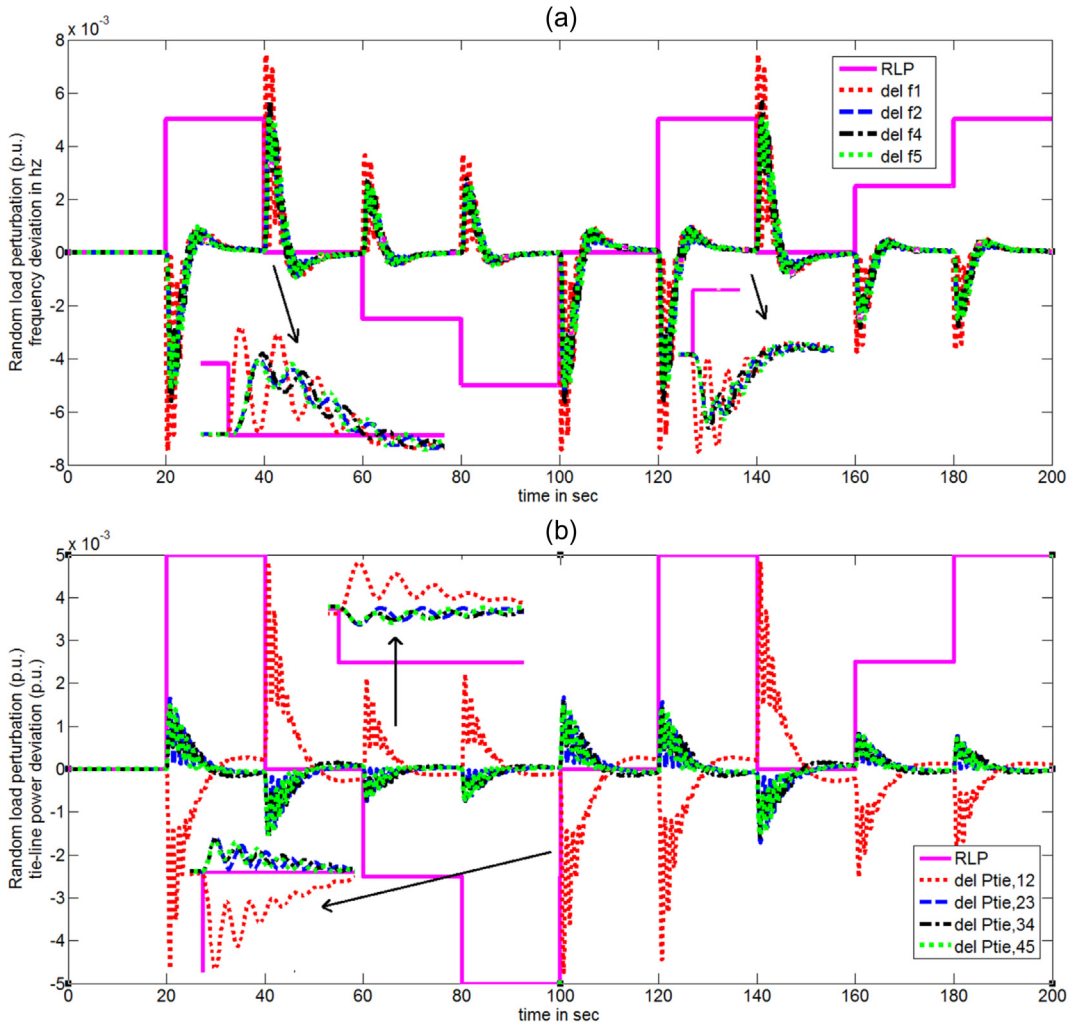


**Fig. 19.** Dynamic behavior of test system-4 subjected to RLP, (a) frequency deviation, (b) tie-line power deviation.

*4.4.2. With GDB and SMES controller*

In this section, the effects of GDB on the system dynamics have been studied with GRC. The optimal PID-controllers designed at Section 4.4.1 are considered in this phase to show its acceptability in LFC area. The dynamic responses of the concerned power system after the load perturbation are shown in Fig. 18 (marked by the blue color). It is obvious that power system oscillations and settling time of frequency and tie-line power will increases with nonlinearities. However, the designed controller is efficient to hold the system stability in this perturbed situation.

To bring out the advantage of SMES controller and to ameliorate the system performance, an optimal coordinated SMES-PID controller is designed using QODSA and placed near at area-1. The closed loop responses with this coordinated controller are presented in Fig. 18 (marked by black color). A close observation of Fig. 18 reveals that proposed coordinated SMES-PID controllers effectively improve the system responses in terms of peak overshoot, undershoot, and settling time and increase the degree of relative stability. This figure also explores the supremacy of proposed coordinated controller in large interconnected power system. Only four figures are presented for justifying the above discussion.

*4.4.3. Robustness analysis of test system-4*

To affirm the robustness of QODSA-tuned PID-controllers for test system-4, a random load profile as shown in Fig. 19 (marked by pink color bold line) is applied to area-1. The change of frequency and tie-line power with this RLP is also shown in Fig. 19. Fig. 19 helps to infer that designed controllers effectively handle this RLP and gives satisfactory performance. The investigation also reveals that power system does not lose its stability under this severe situation.

## 5. Conclusion

In this article, an attempt has been made to improve the dynamic stability of an interconnected power system by introducing a stochastic population-based optimization method called quasi-oppositional differential search algorithm (QODSA). Initially, original DSA is employed to search optimal settings of LFC and then Q-OBL has been added to accelerate the convergence speed and enhance the solution accuracy of DSA. Four different power systems with and without system nonlinearities are considered to demonstrate the efficacy of proposed method under normal and disturbed condition. To establish the superiority of proposed method, the output results are compared with original DSA and other recently published control algorithms for the similar test systems. Simulation results yield that the proposed QODSA-tuned coordinated SMES-PID-controller considerably improves the system performances and enhance the degree of relative stability with system nonlinearities and uncertainties. Finally, the robustness of designed controller has been confirmed with random load perturbation. However, the test systems are needed to study with some advanced controllers and with more nonlinearity.

## Appendix A.

Test system-1: Two-area non-reheat thermal-thermal power system [1–4]

| Parameters | Values | Parameters | Values | Parameters | Values |
|---|---|---|---|---|---|
| f | 60 Hz | $T_{t1} = T_{t2}$ | 0.3 s | $R_1 = R_2$ | 2.4 Hz/p.u MW |
| $P_{r1} = P_{r2}$ | 2000MW | $T_{sg1} = T_{sg2}$ | 0.03 s | $T_{12}$ | 0.545 p.u |
| $K_{ps1} = K_{ps2}$ | 120 Hz/pu MW | $T_{ps1} = T_{ps2}$ | 20 s | $B_1 = B_2$ | 0.425 pu MW/Hz |

Test system-2: Three-unequal-area thermal-thermal power system [2]

| Parameters | Values | Parameters | Values | Parameters | Values |
|---|---|---|---|---|---|
| $B_1$ | 0.3483 | $R_1$ | 3 | $D_1 = D_3$ | 0.015 p.u. Hz |
| $B_2$ | 0.3827 | $R_2$ | 2.73 | $D_2$ | 0.016 p.u. Hz |
| $B_3$ | 0.3529 | $R_3$ | 2.82 | $K_{r1} = K_{r2} = K_{r3}$ | 0.5 |
| $2H_1$ | 0.1667 | $T_{g1}$ | 0.08 s | $T_{t1}$ | 0.4 s |
| $2H_2$ | 0.2017 | $T_{g2}$ | 0.06 s | $T_{t2}$ | 0.44 s |
| $2H_3$ | 0.1247 | $T_{g3}$ | 0.07 s | $T_{t3}$ | 0.3 s |
| $T_{12}$ | 0.2 p.u./Hz | $T_{23}$ | 0.12 p.u./Hz | $T_{31}$ | 0.25 p.u./Hz |

Test system-3: Two-area multi-unit multi-source hydro-thermal power system [35]

| Parameters | Values | Parameters | Values | Parameters | Values |
|---|---|---|---|---|---|
| $P_{r1} = P_{r2}$ | 2000 MW | $T_t$ | 0.3 s | $K_1$ | 1 |
| f | 50 Hz | $T_1$ | 48.7 s | $R_1$ | 2 Hz/p.u. MW |
| $B_1 = B_2$ | 0.425 | $T_2$ | 0.513 s | $R_2$ | 2.4 Hz/p.u. MW |
| $T_{sg}$ | 0.08 s | $T_R$ | 5 s | $T_{12}$ | 0.0707 s |
| $K_{ps}$ | 100 | $T_{ps}$ | 20 | $T_w$ | 1 s |

Test system-4: Five-area thermal power plant [36]

| Parameters | Values | Parameters | Values | Parameters | Values |
|---|---|---|---|---|---|
| $T_{ij}$ | 0.544 | $T_{gi}$ | 0.08 s | $T_{ti}$ | 0.3 s |
| $T_{ri}$ | 10 s | $K_{ri}$ | 0.5 | $R_i$ | 2.4Hz/p.u. MW |
| $T_{ps}$ | 20 s | $K_{ps}$ | 120 Hz/p.u. | $B_i$ | 0.425 p.u. MW/Hz |

## References


[1] E.S. Ali, S.M. Abd-Elazim, Bacteria foraging optimization algorithm based load frequency control for interconnected power system, Int. J. Electr. Power Energy Syst. 33 (2011) 633–638.

[2] S. Padhan, R.K. Sahu, S. Panda, Application of firefly algorithm for load frequency control of multi-area interconnected power system, Electr. Power Compon. Syst. 42 (13) (2014) 1419–1430.

[3] S. Panda, B. Mohanty, P.K. Hota, Hybrid BFOA-PSO algorithm for automatic generation control of linear and nonlinear interconnected power system, Appl. Soft Comput. 13 (12) (2013) 4718–4730.

[4] U.K. Rout, R.K. Sahu, S. Panda, Design and analysis of differential algorithm based automatic generation control for interconnected power system, Ain Shams Eng. J. 4 (3) (2013) 409–421.

[5] S.P. Ghoshal, Optimizations of PID gains by particle swarm optimizations in fuzzy based automatic generation control, Int. J. Electr. Power Syst. Res. 72 (2004) 203–212.

[6] J. Nanda, S. Mishra, L.C. Saikia, Maiden application of bacterial foraging-based optimization technique in multiarea automatic generation control, IEEE Trans. Power Syst. 24 (2) (2009) 602–609.

[7] A.K. Barisal, Comparative performance analysis of teaching learning based optimization for automatic load frequency control of multi-source power systems, Int. J. Electr. Power Energy Syst. 66 (2015) 67–77.

[8] Guha, D., Roy, P.K., and Banerjee, S.: "Optimal Design of Superconducting Magnetic Energy Storage Based Multi-Area Hydro-Thermal System Using Biogeography Based Optimization", In. Proc. of 2014 Fourth Int. Conf. of Emerging Applications of Information Technology, December 2014, pp. 52–57.

[9] S. Patra, S. Sen, G. Ray, Design of robust load frequency controller: $H_\infty$ loop shaping approach, Electr. Power Compon. Syst. 35 (7) (2007) 769–783.

[10] H. Hosseini, B. Tousi, N. Razmjooy, M. Khalilpour, Design robust controller for automatic generation control in restructured power system by imperialist competitive algorithm, IETE J. Res. 59 (6) (2013) 745–752.

[11] S. Debbarma, L.C. Saikia, N. Sinhs, Automatic generation control using two degree of freedom fractional order PID controller, Int. J. Electr. Power Energy Syst. 58 (2014) 120–129.

[12] V. Chandrakala, B. Sukumar, K. Sankaranarayanan, Load frequency control of multi-source multi-area hydro thermal system using flexible alternating current transmission system devices, Electr. Power Compon. Syst. 42 (9) (2014) 927–934.

[13] B.K. Sahu, S. Pati, S. Panda, Hybrid differential evolution particle swarm optimization optimised fuzzy proportional–integral derivative controller for automatic generation control of interconnected power system, IET Gener. Transm. Distrib. 8 (11) (2014) 1789–1800.

[14] A. Demiroren, N.S. Sengor, L.H. Zeynelgil, Automatic generation control by using ANN technique, Electr. Power Compon. Syst. 29 (10) (2001) 883–896.

[15] B. Singh, S. Sharma, Neural network based voltage and frequency controller for isolated wind power generation, IETE J. Res. 57 (5) (2011) 467–477.

[16] Z. Al-Hamouz, N. Al-Musabi, H. Al-Duwaish, S. Al-Baiyat, On the design of variable structure load frequency controllers by tabu search algorithm: application to nonlinear interconnected models, Electr. Power Compon. Syst. 33 (2005) 1253–1267.

[17] S. Prakash, S.K. Sinha, Simulation based neuro-fuzzy hybrid intelligent PI control approach in four-area load frequency control of interconnected power system, Appl. Soft Comput. 23 (2014) 152–164.

[18] W. Yong, J. Zhao, G.M. Dimirovski, Nonlinear adaptive control for multi-machine power system with boiler-generator unit, Int. Trans. Electr. Energy Syst. 25 (2015) 859–875.

[19] R. Yan, Z.Y. Dong, T.K. Saha, R. Majumder, A power systems nonlinear adaptive decentralised controller design, Automatica 46 (2010) 330–336.

[20] L.Y. Sun, J. Zhao, G.M. Dimirovski, Adaptive coordinated passivation control for generator excitation and thyristor controlled series compensation system, Control Eng. Pract. 17 (2009) 766–772.

[21] M. Togifi, M. Alizadeh, S. Ganjefar, M. Alizadeh, Direct adaptive power systems stabilazer design using fuzzy wavelet nural network with self-recurrent consequent part, Appl. Soft Comput. 28 (2015) 514–526.

[22] G.M. Dimirovski, Y.W. Jing, W.L. Li, X.P. Liu, Adaptive backstepping design of TCSC robust nonlinear control for power systems, Intell. Autom. Soft Comput. 12 (2006) 75–87.

[23] Y. Guo, D.J. Hill, Y.Y. Wang, Global transient's stability and voltage regulation for power system, IEEE Trans. Power Syst. 16 (2001) 678–688.

[24] M.R. Sathya, M.M.T. Ansari, Load frequency control using Bat inspired algorithm based dual mode gain scheduling of PI controllers for interconnected power system, Int. J. Electr. Power Energy Syst. 64 (2015) 365–374.

[25] D. Guha, P.K. Roy, S. Banerjee, Application of backtracking search algorithm in load frequency control of multi-area interconnected power system, Ain Shams Eng. J. (2016) (in press).

[26] R.K. Sahu, S. Panda, S. Padhan, Optimal gravitational search algorithm for automatic generation control of interconnected power systems, Ain Shams Eng. J. 5 (2014) 721–733.
[27] K. Zare, M.T. Hagh, J. Morsali, Effective oscillation damping of an interconnected multi-source power system with automatic generation control and TCSC, Int. J. Electr. Power Energy Syst. 65 (2015) 220–230.
[28] M.A. Sahib, A novel optimal PID plus second order derivative controller for AVR system, Eng. Sci. Technol. Int. J. 18 (2015) 194–206.
[29] T.S. Gorripotu, R.K. Sahu, S. Panda, AGC of a multi-area power system under deregulated environment using redox flow batteries and interline power flow controller, Eng. Sci. Technol. Int. J. 18 (2015) 555–578.
[30] P.C. Pradhan, R.K. Sahu, S. Panda, Firefly algorithm optimized fuzzy PID controller for AGC of multi-area multi-source power systems with UPFC and SMES, Eng. Sci. Technol. Int. J. 19 (2016) 338–354.
[31] C.K. Shiva, V. Mukherjee, A novel quasi-oppositional harmony search algorithm for AGC optimization of three-area multi-unit power system after deregulation, Eng. Sci. Technol. Int. J. 19 (2016) 395–420.
[32] D. Guha, P.K. Roy, S. Banerjee, Load frequency control of large scale power system using quasi-oppositional grey wolf optimization algorithm, Eng. Sci. Tech. Int. J. (2016) (in press).
[33] D. Guha, P.K. Roy, S. Banerjee, Load frequency control of interconnected power system using grey wolf optimization, Swarm Evol. Comput. 27 (2016) 97–115.
[34] P. Civicioglu, Transforming geocentric cartesian coordinates to geodetic coordinates by using differential search algorithm, Comput. Geosci. 46 (2012) 229–247.
[35] K.R.M.V. Chandrakala, S. Balamurugan, K. Sankaranarayanan, Variable structure fuzzy gain scheduling based load frequency controller for multi source multi area hydro thermal system, Int. J. Electr. Power Energy Syst. 53 (2013) 375–381.
[36] L.C. Saikia, J. Nanda, S. Mishra, Performance comparison of several classical controllers in AGC for multi-area interconnected thermal system, Int. J. Electr. Power Energy Syst. 33 (2011) 394–401.
[37] A.H. Gandomi, A.H. Alavi, Krill herd: A new bio-inspired optimization algorithm, Commun. Nonlinear Sci. Numer. Simul. 17 (2012) 4831–4845.
[38] B. Liu, Composite differential search algorithm, J. Appl. Math. 2014 (2014) 1–14.
[39] Rahnamayan, S., Tizhoosh, H. R., and Salama, M.M.A.: "Opposition-Based Differential Evolution Algorithms", 2006 IEEE Congress on Evolutionary Computation, Sheraton Vancouver Wall Centre Hotel, Vancouver, BC, Canada, July 16–21, 2006, pp. 2010–17.
[40] C. Zhang, Z. Ni, Z. Wu, L. Gu, A novel swarm model with quasi-oppositional particle, Proc. IEEE 2009 Int. forum on Information Technology Appl., 2009, pp. 325–330.
[41] S.C. Tripathy, T.S. Bhatti, C.S. Jha, O.P. Malik, G.S. Hope, Sampled data automatic generation control analysis with reheat steam turbine and governor dead band effects, IEEE Trans. Power Apparatus Syst. PAS-103 (5) (1984) 1045–1051.
[42] D. Guha, P.K. Roy, S. Banerjee, Oppositional biogeography-based optimisation applied to SMES and TCSC-based load frequency control with generation rate constraints and time delay, Int. J. Power Energy Convers. (2015) (in press).